

Rising surface ozone in China from 2013 to 2017: A response to the recent atmospheric warming or pollutant controls?

Mengmeng Li ^a, Tijian Wang ^{a,*}, Lei Shu ^a, Yawei Qu ^a, Min Xie ^a, Jane Liu ^{a,b}, Hao Wu ^c, Ume Kalsoom ^a

^a School of Atmospheric Sciences, Nanjing University, Nanjing, 210023, China

^b Department of Geography and Planning, University of Toronto, Toronto, Canada

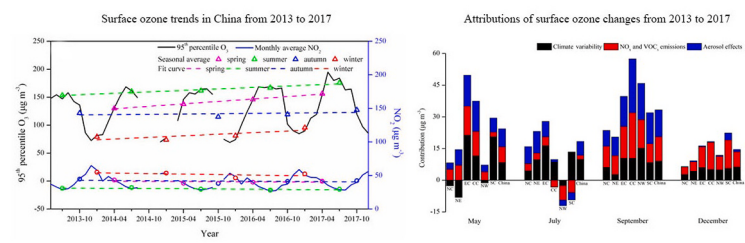
^c School of Environment Sciences, Nanjing University, Nanjing, 210023, China



HIGHLIGHTS

- Air pollution trends are uncovered by satellite data and observations.
- The attributions of surface O₃ changes are more affected by emission changes.
- O₃ response to atmospheric warming is dominant south of 30°N in warm season.
- NO_x and VOC_s control contributed equally as aerosol effect in NCP and East China.

GRAPHICAL ABSTRACT



ARTICLE INFO

Keywords:
Ozone
Atmospheric warming
Emission control
Aerosol effects

ABSTRACT

With the enactment of Air Pollution Action Plan in 2013, the air quality improved in most Chinese cities, except that surface ozone (O₃) increased markedly. Some recent studies have examined this issue and presented controversial opinions, but only focus on summertime ozone increase. This study extends a comprehensive analysis of the influencing factors on China's ozone changes from 2013 to 2017 out of the summer season, combining satellite data, ground measurements and model analyses. The annual trends of air pollutants, e.g., increase in 95th percentile O₃ concentration (+1.4–8.7 µg m⁻³ yr⁻¹), and decreases in fine particulate matter (PM_{2.5}; -4.0~–7.5 µg m⁻³ yr⁻¹) and sulfur dioxide (-2.6~–9.7 µg m⁻³ yr⁻¹) are uncovered by satellite and observational data. Model results show that the attributions of surface O₃ changes from 2013 to 2017 vary spatially and seasonally, and most regions are more affected by emission changes (-9.5–47.0 µg m⁻³) rather than meteorological changes (-8.1–21.3 µg m⁻³). In specific regions and seasons, e.g., south/southwestern and eastern China south of 35°N in May and July, the surface O₃ responses to climate variability could have an equal or even greater importance than emission changes. In these major pollution control regions, e.g. northern and mid-eastern China, the precursor emissions control (11–35%) contributes in the same degree as the changes in aerosol effects (35–38%) to surface ozone enhancement in the warm seasons. More scientific emission controls and climate adaptation strategies are required to attain the synergistic control of atmospheric particulate matter and ozone in China.

* Corresponding author.

E-mail address: tjwang@nju.edu.cn (T. Wang).

1. Introduction

The rapid economic growth in China brought tremendous increase in energy consumption and poor air quality, with particulate matter with aerodynamic diameter less than 2.5 μm ($\text{PM}_{2.5}$) and ozone (O_3) as two key environmental concerns. Quickly responding to the “ $\text{PM}_{2.5}$ Crisis”, the Chinese State Council issued the “Atmospheric Pollution Prevention and Control Action Plan” (hereafter called “Action Plan”) in September 2013 to improve the $\text{PM}_{2.5}$ air quality until 2017. Ten measures were promulgated to cut down the national emissions of sulfur dioxide (SO_2) and nitrogen oxides (NO_x) in the 12th Five-Year Plan (FYP; 2011–2015).

Air quality in most Chinese cities has been improved since then (Li et al., 2019a; Lu et al., 2019; Silver et al., 2018). The annual average concentrations of surface $\text{PM}_{2.5}$, SO_2 and nitrogen dioxide (NO_2) in 74 major cities fell from 72, 40 and 44 $\mu\text{g m}^{-3}$ in 2013 to 47, 17 and 40 $\mu\text{g m}^{-3}$ in 2017 (Bulletin, 2013–2017). But what is worse, ozone, which is a hazardous gas to human health and climate, increased markedly from 139 to 167 $\mu\text{g m}^{-3}$ during 2013–2017 in terms of the maximum daily average 8-h (MDA8) O_3 concentration (Bulletin, 2013–2017). The summertime MDA8 O_3 concentration for the years of 2016–2017 increased by about 20% than that in 2013–2014 (Lu et al., 2018), even although the “Action Plan” has significantly reduced the anthropogenic NO_x emission and abated the winter particulate pollution in China. The past 2017 presented the highest ozone concentration ever recorded in many Chinese cities, with MDA8 O_3 concentrations exceeding the 2nd limit of National Ambient Air Quality Standard (200 $\mu\text{g m}^{-3}$) in 65% of 74 major cities and ozone acting as the primary air pollutant in 43% of the pollution days (Bulletin, 2013–2017). The “seesaw pattern” between $\text{PM}_{2.5}$ and O_3 pollution puts the government into a dilemma and ozone has been the new emphasis of air pollution controls in China.

Tropospheric ozone is produced from a series of photochemical oxidation reactions involving NO_x and volatile organic compounds (VOC_s) (Seinfeld and Pandis, 2006). Some recent studies have examined the rising ozone trend and related it to the control of NO_x and VOC_s emissions (Liu and Wang, 2020b; Wang et al., 2019), the variability in meteorology and synoptic weather conditions (Liu and Wang, 2020a; Lu et al., 2019; Shu et al., 2020), or the interactions with atmospheric particles (Li et al., 2019a; Liu and Wang, 2020b). Lu et al. (2019) explored the source contributions to surface O_3 increase over China in 2016 and 2017; they found that the two-year ozone increase was largely driven by the warmer and drier atmospheric conditions. Liu and Wang (2020a) and Liu and Wang (2020b) examined the roles of meteorological and multi-pollutant emission changes in summer O_3 trends in 2013–2017 using a regional chemical model. They showed that the meteorological influence on ozone could be comparable to that of emission changes; the control of NO_x emission increased O_3 due to the nonlinear $\text{O}_3\text{-NO}_x\text{-VOC}_s$ chemistry, and the reductions of $\text{PM}_{2.5}$ and SO_2 emissions increased O_3 by weakening the aerosol effects. Combining the GEOS-Chem simulation and linear regression analysis, Li et al. (2019a) also found that in the North China Plain (NCP) the rapid decrease in atmospheric $\text{PM}_{2.5}$ was the primary contributor for the summer O_3 increase through weakening the heterogeneous uptake of hydroperoxy radical (HO_2). However, Tan et al. (2020) launched a field campaign in NCP and proposed a contradicting opinion with these model calculations (Li et al., 2019a; Liu and Wang, 2020b). They pointed out that the uptake of HO_2 radical on aerosol surfaces had insignificant impacts on the radical budget in summer and therefore this pathway was not the main reason for ozone increase in this region.

These recent studies presented some interesting and controversial opinions, but only with a focus on summertime ozone increase in China, missing the seasonal variations of ozone trends and their contributors (Wang et al., 2020; Yang et al., 2020). Besides, the complicated interactions between particulate matter and ozone involve the aerosol-radiation effects and aerosol heterogeneous chemistry. Nonetheless, the substantial aerosol-radiation interactions were not taken into account in such off-line simulations (Li et al., 2019a; Liu and Wang,

2020b). Now, the air pollution controls in China have entered a new era, and it is particularly urgent to rethink the key drivers for widespread O_3 increase.

This study aims at extending a more comprehensive analysis of the influencing factors on China's ozone changes from 2013 to 2017 out of the summer season. Satellite data and a five-year surface air quality dataset consisting of O_3 , NO_2 , SO_2 and $\text{PM}_{2.5}$ in 2013–2017 are used to record the recent air quality trends in China. The fully-coupled online Weather Research and Forecasting-Chemistry (WRF-Chem) model with added heterogeneous chemistry is run with varying weather inputs and emissions to quantify the individual roles of climate variability, changes in NO_x and VOC_s emissions and aerosol effects in the recent ozone changes.

2. Methods and data

2.1. Observational data

2.1.1. Surface air quality monitoring data

Surface air pollutants of $\text{PM}_{2.5}$, particulate matter with aerodynamic diameter less than 10 μm (PM_{10}), O_3 , SO_2 , NO_2 and carbon monoxide (CO) in mainland China are routinely monitored and reported hourly by the Chinese National Environmental Monitoring Center (available at <http://www.cnemc.cn/en/>). The nationwide air quality monitoring network was first put into operation in 2013 in 74 major cities (capital cities and major cities in the three largest urban agglomerations in China), and it now included 1597 sites covering 454 cities in mainland China by 2017. In this study, we use the hourly O_3 , NO_2 , SO_2 and $\text{PM}_{2.5}$ data at 447 sites across 74 major cities (Fig. 1) from May 2013 to December 2017 to document the air quality trends in China. The sampling methods and quality assurance procedures comply with the Chinese national ambient air quality monitoring technical regulations HJ/T193-2005.

2.1.2. Satellite data

Tropospheric atmospheric compositions detected from space have been widely used to infer the air pollution and emission trends (Liu et al., 2016; van der A et al., 2008). Here, the Level 3 daily aerosol optical depth (AOD) products derived from Moderate Resolution Imaging Spectroradiometer (MODIS) measurements (accessible at <https://ladsweb.nascom.nasa.gov>) onboard the Terra satellite are used (Remer et al., 2005). The dataset covers the period from 2013 to 2017, with a horizontal resolution of $1^\circ \times 1^\circ$. Levy et al. (2013) estimated that the uncertainty of MODIS AOD product was within $0.05 \pm 20\%$ of AERONET (Aerosol Robotic Network) observations.

Ozone Monitoring Instrument (OMI) onboard the Aura satellite operated by National Aeronautics and Space Administration could provide global observations of ozone and other atmospheric trace gases since October 2004. The data are available from NASA Goddard Space Flight Center (<https://acd-ext.gsfc.nasa.gov>). Monthly gridded tropospheric ozone column (TCO) and tropospheric NO_2 column (TCN) data at $1^\circ \times 1.25^\circ$ resolution measured by OMI from 2013 to 2017 are used here. More details of the datasets can be found in Gaudel et al. (2018). The OMI TCO data compared well with ozonesondes and simulations in terms of the magnitude, seasonal cycle and zonal variations (Ziemke et al., 2006, 2011). The error reported in OMI TCN data was 2.2×10^{15} molecules/cm 2 (Marchenko et al., 2015).

2.1.3. Surface temperature and wind speed in 2013–2017

National Climatic Data Center of U. S. (NCDC; available at www.ncdc.noaa.gov) provides monthly-average climatological variables calculated from the daily observations of Global Historical Climatology Network Daily dataset. Here, monthly summary of surface temperature and wind speed at 46 stations in eastern China (Fig. 1) is used to monitor the inter-annual climate variability from 2013 to 2017.

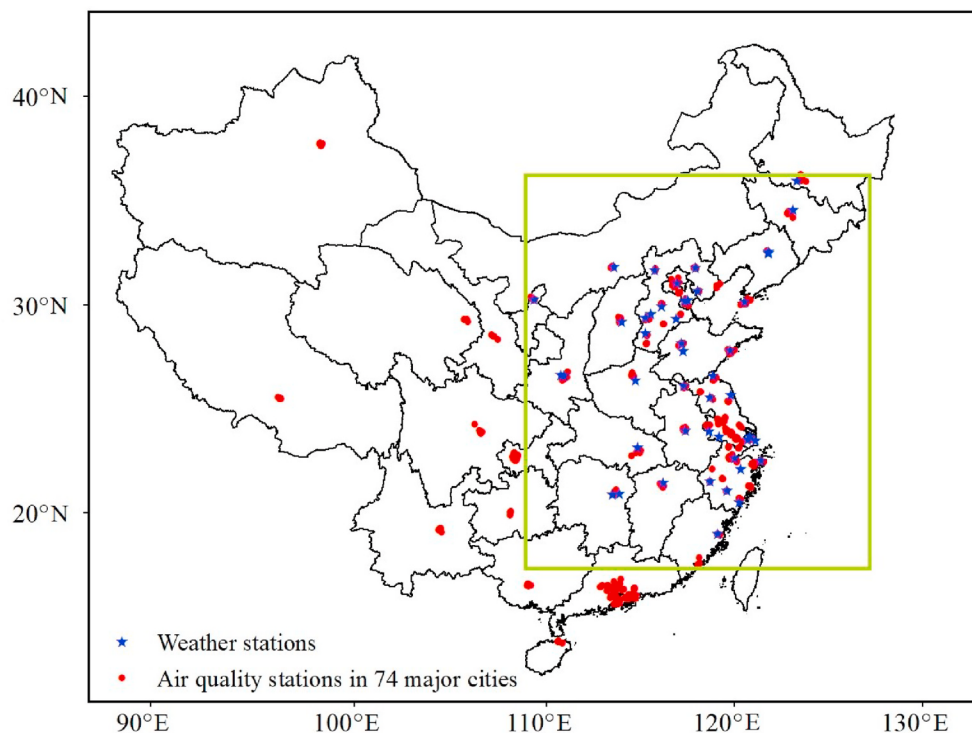


Fig. 1. Surface air quality (red dots) and weather stations (blue stars) in 74 major cities of China. The WRF-Chem modelling domain is marked with green line. (For interpretation of the references to colour in this figure legend, the reader is referred to the Web version of this article.)

2.2. WRF-chem model configurations

This study uses WRF-Chem model version 3.7 to simulate the atmospheric physical, chemical processes and atmospheric compositions in China. The WRF-Chem model is developed by Grell et al. (2002) and it represents the most advanced treatments of coupled meteorology and chemistry. The modeling domain focuses on the eastern China region (Fig. 1). It has a horizontal resolution of $25\text{ km} \times 25\text{ km}$ and totally 98×84 grids. The initial and boundary meteorological fields are obtained from the global final analysis (FNL) data maintained by National Centers for Environmental Prediction. The NCEP/FNL data have a temporal resolution of 6-h and a spatial resolution of $1^\circ \times 1^\circ$. The $0.25^\circ \times 0.25^\circ$ Multi-resolution Emission Inventory for China (MEIC) version 1.3 in 2012–2016 is used to represent the anthropogenic emissions and their changes in China. The emissions of biogenic volatile organic compounds are calculated using Model of Emissions of Gases and Aerosols from Nature, which has been incorporated online in WRF-Chem (Guenther et al., 2006).

Numerous gas-phase and aerosol-phase chemical reaction mechanisms have been incorporated in the WRF-Chem model. In this study, the gas-phases chemistry is described by the lumped CBMZ chemical mechanism developed by Zaveri and Peters (1999). The aerosol chemistry is described by the MOSAIC aerosol scheme configured with 4 sectional aerosol bins (Zaveri et al., 2008). The optimal physical parameterization schemes included in the simulation contain the Goddard short-wave radiation scheme (Chou and Suarez, 1999) and RRTM long-wave radiation scheme (Gallus and Bresch, 2006) to calculate radiation transfer in the atmosphere, the YSU boundary layer parameterization scheme (Noh et al., 2003) to characterize the boundary layer structure, the Noah land surface model (Ek et al., 2003) to describe the land-atmosphere interactions, and the Lin microphysics scheme (Lin et al., 1983) to describe the cloud microphysical processes.

Following Li et al. (2017b) and Lou et al. (2014), new heterogeneous reactions (R1~R21 in Table S1) on particles have been incorporated into the MOSAIC aerosol module. The uptake coefficients are determined

from the recent laboratory results (Bauer et al., 2004; Bedjanian et al., 2013; DeMore, 2000; Dentener et al., 1996; Evans and Jacob, 2005; Huang et al., 2014; Jacob, 2000; Lei et al., 2004; Liu et al., 2008; Pradhan et al., 2010; Rogaski et al., 1997; Saathoff et al., 2001; Slade and Knopf, 2013; Thornton et al., 2008; Zhang and Carmichael, 1999; Zheng et al., 2015) (Table S1). The modified WRF-Chem model performance has been evaluated in our previous works (Li et al., 2017b, 2018, 2019c), showing that it could reflect the atmospheric pollution characteristics in China.

2.3. Numerical experimental designs

Eleven WRF-Chem simulations are designed in Table 1. The base simulation B0 is driven by the global NCEP/FNL meteorological data in 2017 and the MEIC inventory in 2016, as a substitution for the anthropogenic emissions in 2017. The aerosol effects on ozone through radiation interactions and heterogeneous chemistry are also included in B0. The B1 simulation is the same as B0, but driven by the global NCEP/FNL meteorological data in 2013 and the MEIC inventory in 2012, as a substitution for the anthropogenic emissions in 2013. The differences between B0 and B1 simulations are calculated to show the total ozone changes from 2013 to 2017 due to the changes in meteorology, anthropogenic NO_x and VOC_s emissions and aerosol effects. We then conduct another two sensitivity simulations with the anthropogenic emissions of NO_x and VOC_s set to the 2013 level (E1) and the meteorological inputs set to the global NCEP/FNL data in 2013 (C1). E1 and C1 are designed to calculate the impacts of changes in anthropogenic NO_x and VOC_s emissions (B0–E1) and meteorological conditions (B0–C1) on surface ozone changes between 2013 and 2017.

In addition to directly altering the emissions of ozone precursors—NO_x and VOC_s, the emission controls might affect ozone concentrations through indirectly disturbing the aerosol effects. The other simulations (A1~A7) are designed with/without the aerosol effects under current/past emission conditions to calculate the impacts of changes in aerosol effects (including aerosol radiative effects and

Table 1

WRF-Chem numerical experiments in this study.

Cases	Meteorological inputs	NO _x and VOC _s emissions	Emissions for others	Radiative feedback	Heterogeneous chemistry	Aims
Base simulation						
B0	FNL 2017	MEIC 2016	MEIC 2016	✓	✓	B0 and B1 are designed to simulate the total O ₃ changes due to the changes in climate, NO _x and VOC _s emissions and aerosol effects from 2013 to 2017 (B0–B1)
B1	FNL 2013	MEIC 2012	MEIC 2012	✓	✓	
NO _x and VOC _s emissions						
E1	FNL 2017	MEIC 2012	MEIC 2016	✓	✓	E1 is designed to simulate the O ₃ changes due to NO _x and VOC _s emissions changes from 2013 to 2017 (B0–E1)
Climate						
C1	FNL 2013	MEIC 2016	MEIC 2016	✓	✓	C1 is designed to simulate the O ₃ changes due to climate variability from 2013 to 2017 (B0–C1)
Aerosol effects						
A1	FNL 2017	MEIC 2016	MEIC 2016	✗	✗	A1 is designed to simulate the aerosol effects on O ₃ under current emission conditions (B0–A1)
A2	FNL 2017	MEIC 2012	MEIC 2012	✓	✓	A2 and A3 are designed to simulate the aerosol effects on O ₃ under past emission conditions (A2–A3)
A3	FNL 2017	MEIC 2012	MEIC 2012	✗	✗	
A4	FNL 2017	MEIC 2016	MEIC 2016	✓	✗	A4 is designed to simulate the impacts of aerosol heterogeneous chemistry on ozone under current emission conditions (B0–A4)
A5	FNL 2017	MEIC 2012	MEIC 2012	✓	✗	A5 is designed to simulate the impacts of aerosol heterogeneous chemistry on ozone under past emission conditions (A2–A5)
A6	FNL 2017	MEIC 2016	MEIC 2016	✗	✓	A6 is designed to simulate the impacts of aerosol radiative effects on ozone under current emission conditions (B0–A6)
A7	FNL 2017	MEIC 2012	MEIC 2012	✗	✓	A7 is designed to simulate the impacts of aerosol radiative effects on ozone under past emission conditions (A2–A7)

aerosol heterogeneous chemistry) on ozone between 2013 and 2017. For example, the total aerosol impacts on ozone concentrations could be expressed as B0–A1 under current emission conditions, and A2–A3 under past emission conditions. Thus, the aerosol effects on ozone changes between 2013 and 2017 could be calculated as the differences between B0–A1 and A2–A3. Therein, A4~A7 simulations are designed to distinguish the separate impacts of aerosol radiative effects and aerosol heterogeneous chemistry on surface ozone changes between 2013 and 2017.

3. Results and discussions

3.1. Trends for air pollutant emissions in the recent decade

Fig. 2 shows the annual trends of anthropogenic emissions in mainland China from the MEICv1.3 inventory and recent references (Kang et al., 2016; NBSC, 2004–2016; Xia et al., 2016) during 2002–2016. The rapid economic expansion in China is powered by a

coal-fueled energy consumption (Fig. 2a), and an increase in air pollutant emissions seems inevitable until the 11th FYP (2006–2010; Fig. 2b).

After 2006, the emissions of SO₂ was cut down along with the nationwide use of flue gas desulfurization (FGD) systems in power plants (from 83% to 99% (Li et al., 2017a)) and the decommissioning of small units. The annual decrease rate of SO₂ emission was $-7.0\% \text{ yr}^{-1}$ for the period 2008–2016, according to the MEIC v1.3 dataset. The national emission of PM_{2.5} remained nearly unchanged in 2008–2012 and decreased quickly at a rate of $-7.9\% \text{ yr}^{-1}$ in 2012–2016 (MEIC v1.3), mainly due to the widespread installation of the FGD systems and other particulate removal technologies in the electricity and cement industries. The control of NO_x emission lagged behind that of SO₂. The NO_x emission increased continuously by $+5.3\% \text{ yr}^{-1}$ from 2008 to 2012, and since then the promotion of denitrification techniques (e.g., Selective Catalytic Reduction techniques) for power, industry and transportation sectors effectively reduced the NO_x emissions by 22.8% ($-5.7\% \text{ yr}^{-1}$) from 2012 to 2016 (MEIC v1.3). For VOC_s, however, the

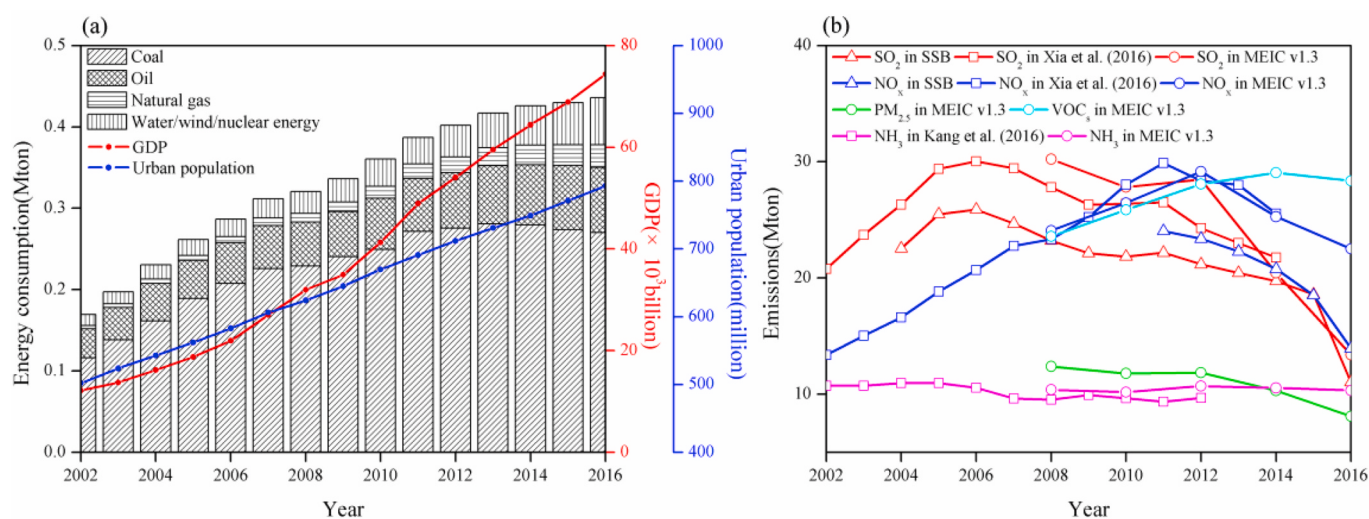


Fig. 2. Trends of (a) energy consumption (available at <http://www.stats.gov.cn/>), and (b) anthropogenic emissions of main air pollutants in China from MEICv1.3 and recent references during 2002–2016.

emission reductions due to the improved vehicle emission standards and clean energy (Li et al., 2017a) were counteracted by the large emission increases from processes and organic solvent use, resulting in a continuous VOC emission increase by $4.8\% \text{ yr}^{-1}$ from 2008 to 2012 and by $0.2\% \text{ yr}^{-1}$ from 2012 to 2016 (MEIC v1.3). During the 12th FYP, significant decreases in the anthropogenic emissions of NO_x , SO_2 and $\text{PM}_{2.5}$ were found in China, except for VOCs (Fig. S1). Concurrently, the ratio of NO_x emission to VOCs emission on the national level decreased from 1.04 to 0.79 between 2012 and 2016.

3.2. Air pollutants trends in 2013–2017 from satellite and ground observations

Fig. 3 shows the annual trends of MODIS AOD, and OMI TCO and TCN in China from 2013 to 2017. The emission trends for $\text{PM}_{2.5}$ and NO_2 in China are confirmed by satellite observations. Space-based measurements of AOD and TCN reveal a rapid decrease of tropospheric $\text{PM}_{2.5}$ ($-3.3\% \text{ yr}^{-1}$) and NO_2 ($-3.2\% \text{ yr}^{-1}$) in China from 2013 to 2017, as a consequence of the reduced emissions with stricter pollution control measures. The highly industrialized Beijing-Tianjin-Hebei (BTH) region ($34\text{--}41^\circ\text{N}$, $112\text{--}120^\circ\text{E}$) shows the highest AOD and TCN values, and the largest rate of decrease ($-5.7\% \text{ yr}^{-1}$ and $-9.9\% \text{ yr}^{-1}$), followed by the Yangtze River Delta (YRD) region ($28\text{--}33^\circ\text{N}$, $118\text{--}123^\circ\text{E}$; $-4.0\% \text{ yr}^{-1}$ and $-5.8\% \text{ yr}^{-1}$). The spatial distribution of TCO trend ($+0.4\% \text{ yr}^{-1}$), however, is much more uniform than that of AOD and TCN, ascribed to the long lifetime and complex production processes of tropospheric ozone (Seinfeld and Pandis, 2006). Distinct seasonal differences are observed for TCO trends, with an increase in mid-eastern China and its surrounding sea areas in spring and large inter-annual fluctuations in autumn (Fig. S2). In summer and winter with extremely high and low O_3 , the TCO trends are insignificant. Similar air pollution trends from satellite are also confirmed by recent reports (Li, 2020; Liu et al., 2016; Zhou et al., 2019).

Fig. 4 and Fig. 5 illustrate the trends of monthly-average surface $\text{PM}_{2.5}$, SO_2 and NO_2 concentrations and 95th percentile O_3 concentrations in 74 major cities of China during the 2013–2017 period. The sites

with missing data more than 25% are not used in the computations. The seasonal-specific linear regression lines indicate that the surface $\text{PM}_{2.5}$ concentrations decreased at a rate of -5.0 , -4.0 , -6.2 and $-7.5 \mu\text{g m}^{-3} \text{ yr}^{-1}$, respectively, in spring, summer, autumn and winter from 2013 to 2017. The annual trends for $\text{PM}_{2.5}$ are statistically significant with P-value below 0.05. The results confirm the recently reported surface $\text{PM}_{2.5}$ trends (Silver et al., 2018; Zheng et al., 2017) across China. The observed decrease in $\text{PM}_{2.5}$ is most likely due to the reduced SO_2 emissions and thereby atmospheric SO_2 levels in mainland China, which ranges from $-2.6 \mu\text{g m}^{-3} \text{ yr}^{-1}$ in summer to $-9.7 \mu\text{g m}^{-3} \text{ yr}^{-1}$ in winter. The declining trends of surface $\text{PM}_{2.5}$ and SO_2 concentrations between 2013 and 2017 are visible at more than 80% of the sites, with faster reductions around the pollution control target cities, e.g., the BTH (-8.6 and $-9.9 \mu\text{g m}^{-3} \text{ yr}^{-1}$ for $\text{PM}_{2.5}$ and SO_2) and YRD (-7.2 and $-3.8 \mu\text{g m}^{-3} \text{ yr}^{-1}$ for $\text{PM}_{2.5}$ and SO_2) metropolitan areas (Fig. 5).

In contrast with that of $\text{PM}_{2.5}$ and SO_2 , the 95th percentile O_3 concentrations show a clearly increasing trend with a seasonal cycle, at a rate of 8.7 , 5.6 , 1.4 and $5.5 \mu\text{g m}^{-3} \text{ yr}^{-1}$, respectively, in spring, summer, autumn and winter from 2013 to 2017. The largest increase of O_3 between 2013 and 2017 appears in the mostly populated YRD ($6.2 \mu\text{g m}^{-3} \text{ yr}^{-1}$) and BTH ($3.4 \mu\text{g m}^{-3} \text{ yr}^{-1}$) regions of eastern China. The O_3 increase in the Pearl River Delta (PRD) region of southern China is insignificant, except in the spring season (Fig. 5). The rising O_3 levels are consistent with recent studies, who estimated that the MDA8 O_3 concentrations in China increased by $4.6 \mu\text{g m}^{-3} \text{ yr}^{-1}$ in 2015–2017 (Silver et al., 2018), and $4.9 \mu\text{g m}^{-3} \text{ yr}^{-1}$ for the warm seasons in 2016–2017 than the years of 2013–2014 (Lu et al., 2018). The surface NO_2 trends are more variable. There is no clear trend in the seasonal mean NO_2 concentrations ($-0.3\text{--}-0.9 \mu\text{g m}^{-3} \text{ yr}^{-1}$), which has already been found by Silver et al. (2018). The trends for surface NO_2 concentrations show large spatial inhomogeneity and even opposite trends for adjacent areas (Fig. 5), which could be possibly because of the high reactivity and short lifetime of NO_2 .

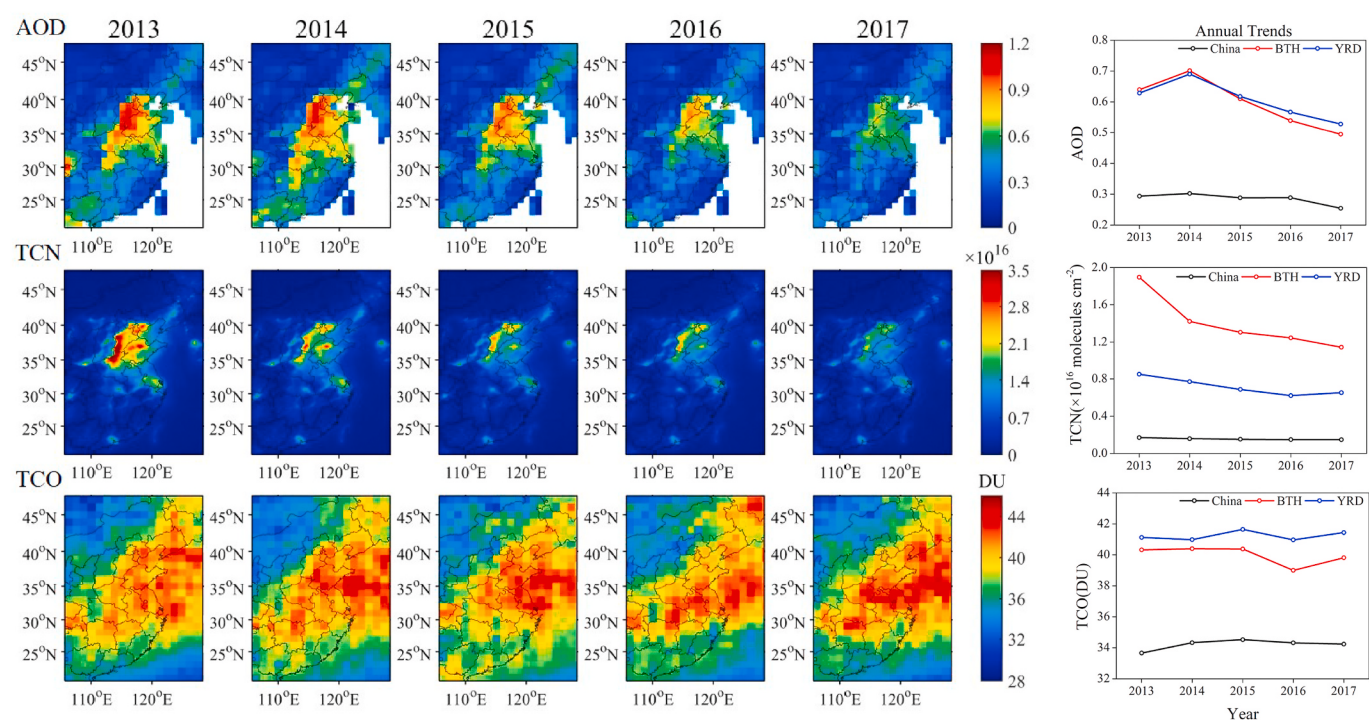


Fig. 3. Annual trends of AOD (upper panels), TCN (unit: $\times 10^{16} \text{ molecules cm}^{-2}$, middle panels) and TCO (unit: DU; bottom panels) in China from satellite observations during 2013–2017.

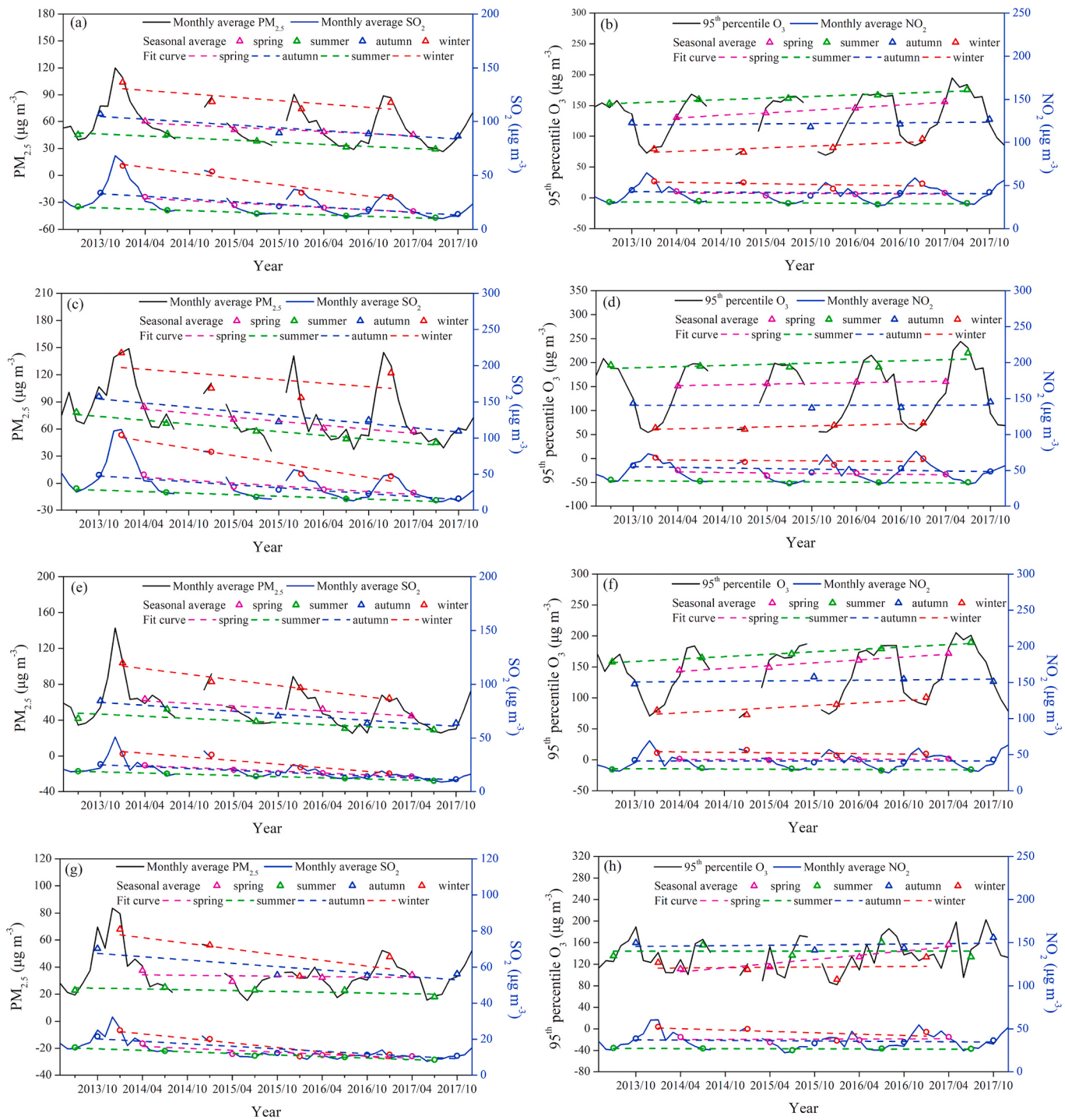


Fig. 4. Annual trends of the monthly-average (solid lines) and seasonal-average (hollow triangles) values for surface PM_{2.5}, SO₂ and NO₂ concentrations and 95th percentile O₃ concentrations during 2013–2017 in (a, b) 74 major cities of China, (c, d) BTH region, (e, f) YRD region and (g, h) PRD region.

3.3. Attributions of surface ozone changes in China from 2013 to 2017

The 2-year model results allow us to analyze the factors contributing to surface ozone changes from 2013 to 2017. We focus on the eastern China region (Fig. 1) in four representative months (May, July, September and December), when and where the most dramatic air quality changes occur.

Model evaluations show that the WRF-Chem model faithfully captures the spatial and seasonal patterns of observed PM_{2.5}, NO₂ and O₃ levels (Fig. 6), with an annual-average correlation coefficient (*R*) of

0.71, 0.55 and 0.72, a mean bias (MB) of -14.30, -15.49 and 5.17 µg m⁻³, and a normalized mean bias (NMB) of -30.64, -38.43 and 7.10% for PM_{2.5}, NO₂ and O₃ (Table 2). Both the simulations and observations exhibit elevated air pollutant concentrations in eastern China, but with higher O₃ level in the warm seasons and oppositely higher PM_{2.5} and NO₂ concentrations in winter. Underestimation of surface PM_{2.5} (-39.42~-8.64%; Table 2) usually exist in most seasons, which may be associated with the error in emission inventory or the absence of secondary organic aerosol in MOSAIC aerosol chemistry, which could contribute 16% to PM_{2.5} mass concentration in China (Zhao et al.,

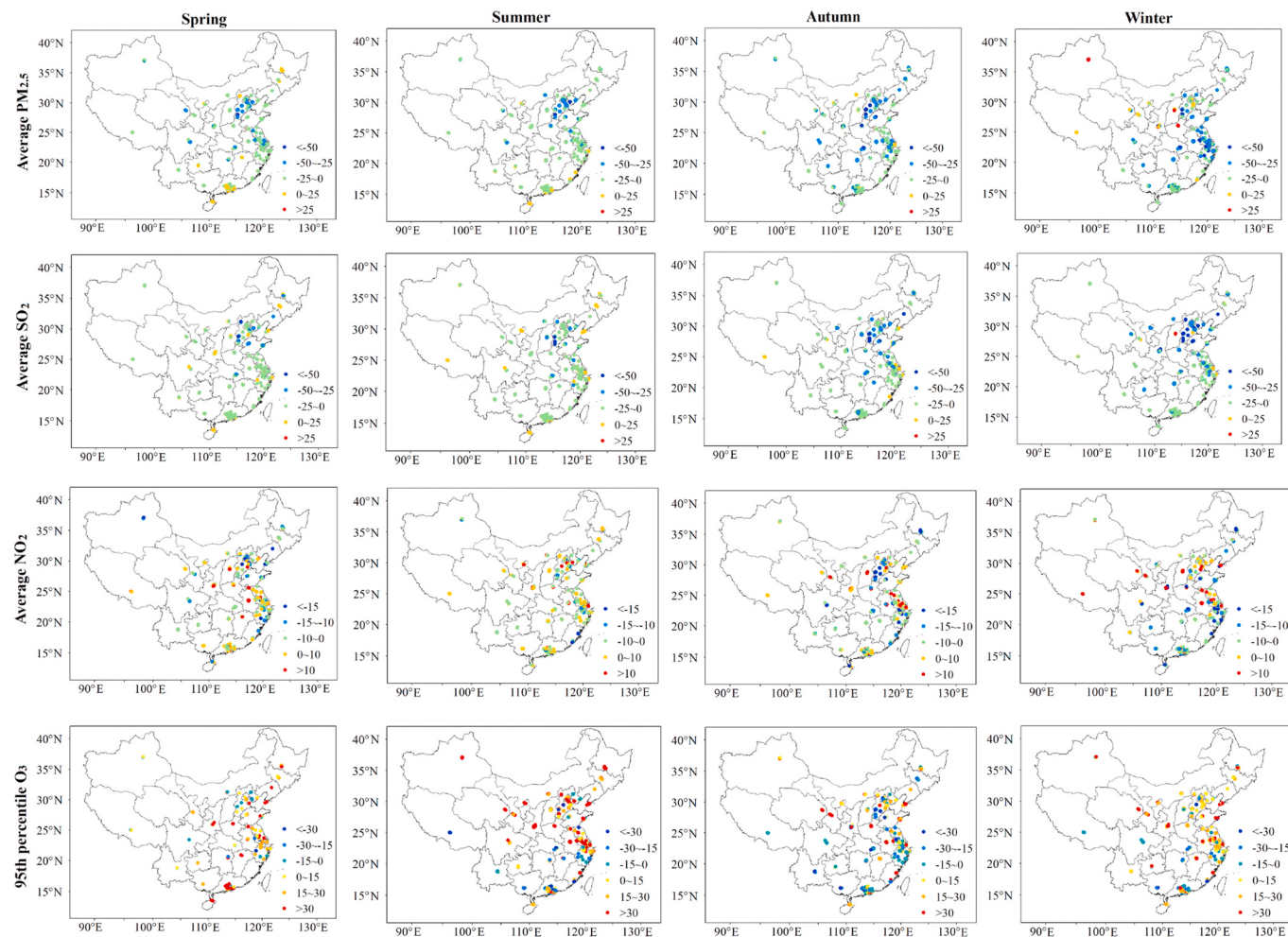


Fig. 5. Spatial distributions of the absolute changes of surface average PM_{2.5}, SO₂ and NO₂ concentrations and 95th percentile O₃ concentrations (unit: $\mu\text{g m}^{-3}$) in 2017 relative to that of 2013 during four seasons.

2016).

The simulated surface O₃ changes on the nationwide level range from 14.3 to 18.3 $\mu\text{g m}^{-3}$ for different seasons from 2013 to 2017, with a hotspot area near northern and eastern China (Fig. 7). Table 3 compares the simulated surface O₃ changes with observations at the air quality monitoring network. The model generally captures the seasonal patterns of increasing surface O₃ trends in 2013–2017, with stronger surface O₃ increases in the spring-summer-autumn seasons. But the model results commonly overestimate the magnitudes of surface O₃ changes by -1.59, 7.97, 7.63 and 2.80 $\mu\text{g m}^{-3}$ on the nationwide level for May, July, September and December, respectively (Table 3). Regionally, the surface O₃ changes are well predicted in heavily polluted northern China for most seasons (+1.64 $\mu\text{g m}^{-3}$ averagely), positively biased in central and eastern China (+10.48 $\mu\text{g m}^{-3}$ averagely), and negatively biased in northeastern and northwestern China in particularly for May and July (-4.18 $\mu\text{g m}^{-3}$ averagely). We then quantitatively separate the key drivers for surface ozone changes in 2017 relative to 2013 to the changes in meteorology, NO_x and VOC_s emissions and aerosol effects (Figs. 7 and 8). The model results show that the attributions of surface O₃ changes vary spatially and seasonally, and that most of these regions are more affected by emission changes (-9.5–47.0 $\mu\text{g m}^{-3}$) rather than meteorological changes (-8.1–21.3 $\mu\text{g m}^{-3}$, Fig. 7). A more detailed analysis of the influencing factors on surface ozone changes in China from 2013 to 2017 is discussed below.

3.3.1. Responses of surface ozone changes to atmospheric warming

The China Climate Bulletin reported a higher atmospheric temperature in 2017 than the normal levels for all seasons. Li et al. (2019b) revisited the temperature trends in China between 1980 and 2017 and also found that 2017 was the warmest year since 1980. We analyze the monthly weather summary at 46 surface stations in China and find a continuous increase for temperature (particularly in spring and winter) and a slow decrease for wind speed from 2013 to 2017 (Fig. S3 and Fig. S4). A sensitivity simulation C1 is conducted with fixed anthropogenic emissions to test the sensitivity of ozone to climate variability between the 2 years (Table 1). The simulated surface temperature changes from 2013 to 2017 by WRF-Chem agree well with observations in terms of spatial characteristics and magnitudes (Fig. 9), with a R of 0.83, 0.72, 0.75 and 0.66 and a MB of -0.42, -0.27, +0.09 and -0.17 °C, respectively, in May, July, September and December (Table 4). Surface temperature in 2017 is higher than 2013 in northern and eastern China, accompanied by drier atmospheric humidity and higher wind speed. Similar atmospheric warming is also found for central and southern China in autumn and winter, but with more complex seasonal variations for humidity and wind speed (Fig. 9).

The atmospheric warming and changes in other associated weather conditions in 2017 can alter tropospheric ozone concentrations by modulating the chemical kinetic, dynamic processes or biogenic emissions. Warmer temperatures often coincide with other meteorological conditions favorable to O₃ production, such as stagnation air and reduced cloud cover (Vukovich, 1995). High humidity associated with

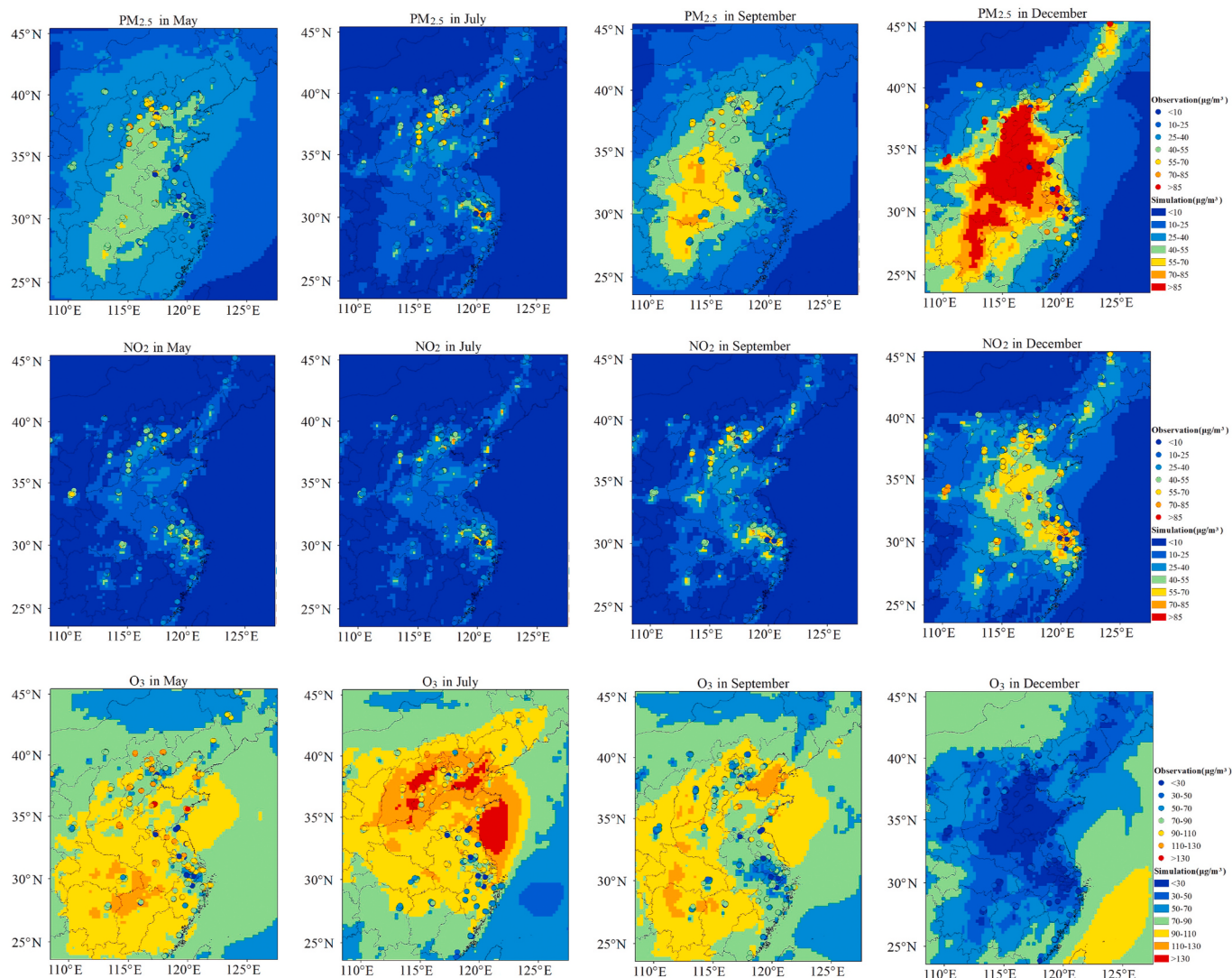


Fig. 6. Spatial pattern comparisons of the simulated surface average PM_{2.5} (upper panels), NO₂ (middle panels) and O₃ (bottom panels) concentrations in B0 experiment with observations in four seasons of 2017.

Table 2

Statistical evaluations for the simulated surface NO₂, O₃ and PM_{2.5} concentrations ($\mu\text{g m}^{-3}$) in four seasons of 2017 in the B0 simulation.

Species	NO ₂			O ₃			PM _{2.5}		
	Period	R	MB	NMB	R	MB	NMB	R	MB
May	0.49	-10.55	-28.87	0.43	-12.44	-12.72	0.40	-17.11	-39.42
July	0.37	-7.72	-26.55	0.51	13.78	15.56	0.69	-11.31	-33.86
September	0.56	-14.06	-37.48	0.61	8.34	11.30	0.54	-3.11	-8.64
December	0.59	-21.96	-37.68	0.45	11.13	36.30	0.68	-15.98	-21.52
Annual	0.55	-15.49	-38.43	0.72	5.17	7.10	0.71	-14.30	-30.64

larger cloud cover and atmospheric instability slow down the photochemical process and accelerate O₃ deposition on water droplets (Camalier et al., 2007; Davis et al., 2011). Fig. 10 establishes the relationship between the simulated surface O₃ changes and changes in temperature, humidity and wind speed between 2013 and 2017 in China. Using linear fitting method, we find that the changes in surface O₃ concentrations are positively associated with that of atmospheric temperature, but strongly negatively correlated to humidity and wind speed for most seasons, with an average response rate of 0.15 $\mu\text{g m}^{-3}/^{\circ}\text{C}$, -1.06 $\mu\text{g m}^{-3}/(\text{mg kg}^{-1})$ and -6.16 $\mu\text{g m}^{-3}/(\text{m s}^{-1})$. Our findings are consistent with some recent modeling (Sillman and Samson, 1995; Zeng et al., 2008) and observational (Bloomer et al., 2009;

Camalier et al., 2007; Davis et al., 2011) studies.

We examine the meteorological changes (Fig. 9) and their possible impacts on ozone levels from 2013 to 2017 (Figs. 7 and 8). The meteorological influence on surface ozone changes varies by region and season, ranging from -8.1 to 21.3 $\mu\text{g m}^{-3}$. In most cases, such warmer and drier climatic conditions in 2017 accelerate the ozone production rates in China, leading to a drastic increase in the surface O₃ mixing ratio by 6.3–9.9 $\mu\text{g m}^{-3}$ on the nationwide average. An exception is that the meteorological influence on ozone is negative in northern and northeastern China of May, showing an O₃ decrease by -2.6 and -8.1 $\mu\text{g m}^{-3}$, respectively. The significantly lower air temperature in May over most parts of Inner Mongolia and northeastern China (Fig. 9) could explain

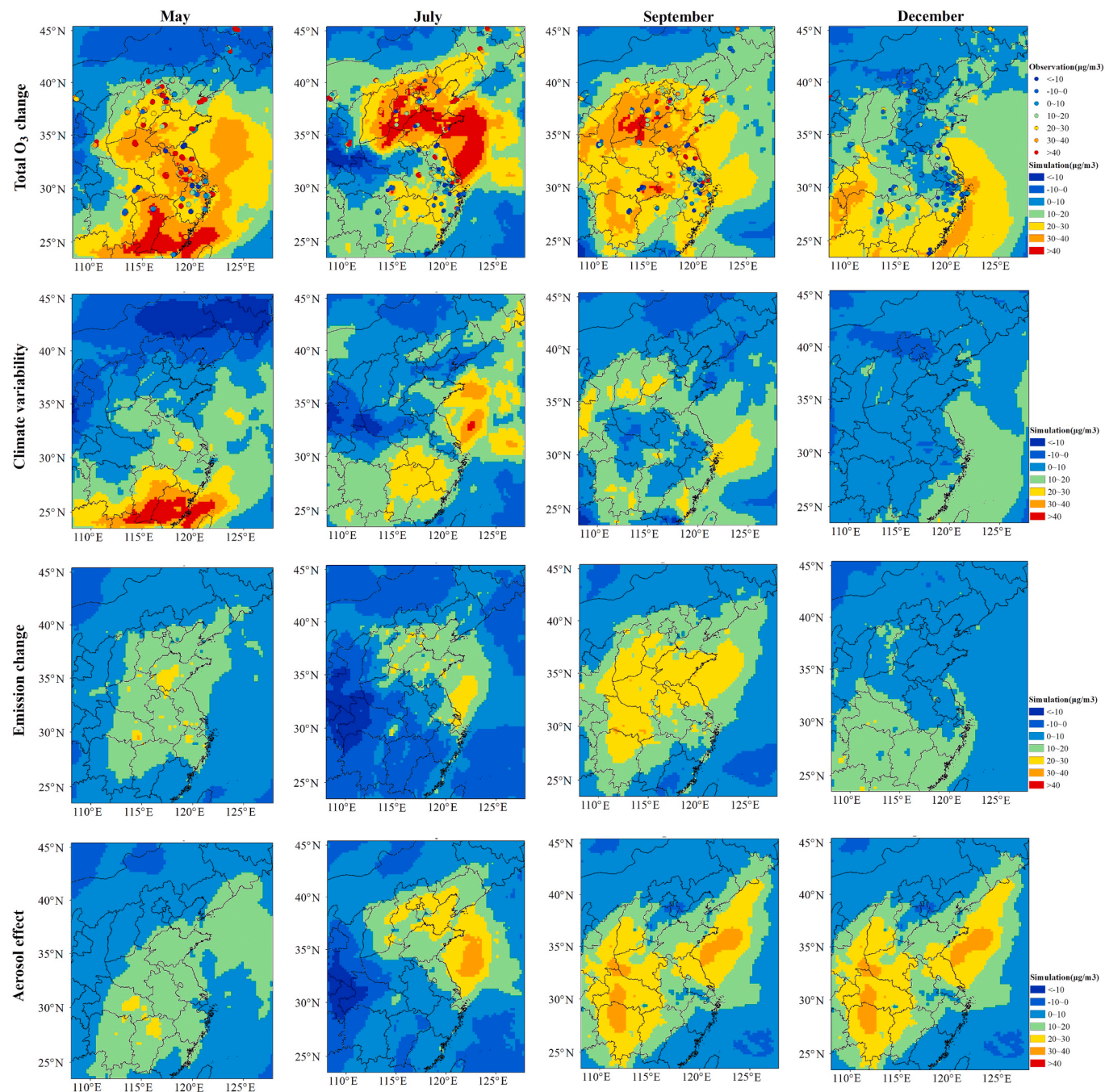


Fig. 7. Modelled surface O₃ changes (upper panels) from 2013 to 2017 attributed to climate variability (second panels), changes in anthropogenic NO_x and VOC_s emissions (third panels), and changes in aerosol effects (bottom panels). Observed surface O₃ changes are marked with solid circles in the first panels.

Table 3

Comparisons of the simulated and observed surface ozone changes ($\mu\text{g m}^{-3}$) in four seasons between 2013 and 2017 on the regional level.

Region ^a	May		July		September		December	
	Obs	Sim	Obs	Sim	Obs	Sim	Obs	Sim
China	27.24	25.65	17.24	25.21	12.06	19.69	4.33	7.13
NC	28.18	20.86	26.89	34.83	21.20	27.76	6.96	6.32
EC	25.79	33.32	7.24	22.37	7.98	19.13	3.38	9.78
CC	25.33	29.56	19.09	27.99	3.90	25.81	1.86	10.48
NE	40.43	3.60	32.86	16.51	17.16	13.02	9.38	7.86
NW	8.67	12.55	26.96	8.83	-8.05	19.40	-1.52	10.70
SC ^b	-	-	-	-	-	-	-	-

^a NC: Northern China; NE: Northeastern China; EC: Eastern China; CC: Central China; NW: Northwestern China; SC: Southern and Southwestern China.

^b Observation sites are not available in SC of the modelling domain (Fig. 1).

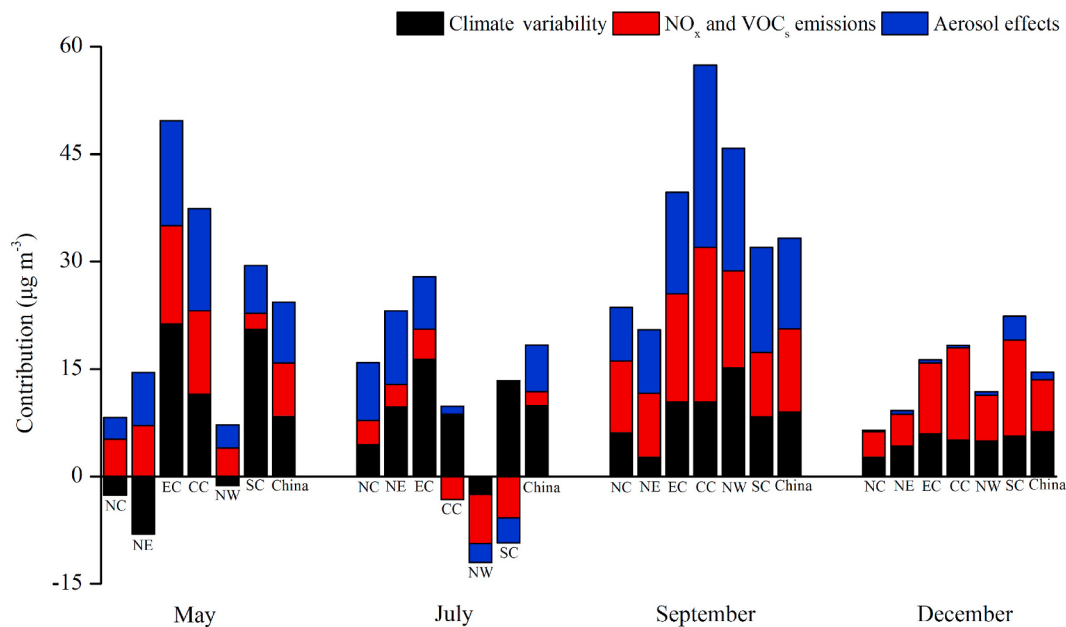


Fig. 8. Modelled surface O_3 changes from 2013 to 2017 due to climate variability, changes in anthropogenic NO_x and VOC_s emissions, and changes in aerosol effects in typical regions of China. NC: Northern China; NE: Northeastern China; EC: Eastern China; CC: Central China; NW: Northwestern China; SC: Southern and Southwestern China.

the large O_3 decline due to meteorological variations.

In specific regions and seasons, e.g., south/southwestern and eastern China regions south of 35°N in May and July, the surface O_3 responses to climate variability could have an equal or even greater impact than emission changes (Fig. 8). For example, the extremely lower humidity (more than 2 mg kg^{-1}) in May of 2017 over south/southwestern China (Fig. 9) results in an increase of surface O_3 by as much as $20.6 \mu\text{g m}^{-3}$, while the warmer air together with lower wind speed in July result in an O_3 enhancement by $13.4 \mu\text{g m}^{-3}$. The increased ozone in response to extremely low humidity might be due to the enhanced ozone photochemical removal and ventilation in presence of high humidity (Camarier et al., 2007; Davis et al., 2011), which has already been observed in Europe (Zoran et al., 2020) and China (Cheng et al., 2010). Similarly, the large increase of ozone ($16.3 \mu\text{g m}^{-3}$) over eastern China in July from 2013 to 2017 is primarily driven by the climate variability featured by moderately warmer atmosphere with lower humidity and wind speed.

The model results with year-specific meteorology highlight the significant role of climate variability in ozone variations, but could not yet fully explain the substantial O_3 increases in the heavily polluted northern and eastern China regions. The residual gaps between the simulated and observed ozone changes indicate a possible ozone enhancement dominated by the recent pollutant controls.

3.3.2. Impacts of recent pollutant controls on surface ozone changes

The recent emission controls in China might affect ozone concentrations through directly altering the emissions of ozone precursors— NO_x and VOC_s , or through indirectly disturbing the aerosol effects. Several sensitivity simulations (E1 and A1~A7; Table 1) are conducted with varying pollutant emissions but with a single year's meteorology to calculate the impacts of atmospheric pollutant controls on surface O_3 changes in China between 2013 and 2017. The spatial patterns of surface ozone increases calculated in northern and eastern China are in good agreement with the simulated ozone changes due to the NO_x and VOC_s emissions controls and aerosol effects (Fig. 7), which are therefore believed to be the main drivers of ozone increases for these major pollution control regions. Impacts of the emission changes in recent years on surface ozone and their principal causes vary geographically and seasonally, ranging by $1.9\text{--}11.6 \mu\text{g m}^{-3}$ due to the

NO_x and VOC_s emissions changes and by $1.0\text{--}12.7 \mu\text{g m}^{-3}$ due to the changes in aerosol effects on the nationwide average for different seasons (Fig. 8). The relative contribution of NO_x and VOC_s emissions changes to the total surface O_3 changes becomes increasingly significant in spring, autumn and winter (31–50%), when the anthropogenic emissions and their reductions are most highest. Whereas, the relative contribution of aerosol effects show opposite seasonal trends, which is more significant in spring-summer-autumn seasons (35–38%) and is negligible (7%) in winter, despite the substantial decrease in aerosol concentrations (Fig. S5).

The model driven by the estimated changes in anthropogenic NO_x (-22.8%) and VOC_s ($+0.9\%$) emissions, along with the reduced NO_x/VOC_s emission ratio from 1.04 to 0.79, results in an increase of surface O_3 mixing ratios for most regions throughout the year ($-6.8\text{--}21.5 \mu\text{g m}^{-3}$ by region and season), especially in the highly polluted northern and mid-eastern China regions where larger emission reductions occurred in the past few years. Otherwise, a significant decrease in surface O_3 concentrations is found across a large area of southern, central and northwestern China in July ($-6.8\text{--}-3.2 \mu\text{g m}^{-3}$). This regional and seasonal discrepancy might be explained by the nonlinear $\text{O}_3\text{-NO}_x\text{-VOC}_s$ chemistry and different ozone chemical regimes in China's urban/rural areas (typically VOC_s -limited in cities and NO_x -limited in rural area) and in winter/summer (typically VOC_s -limited in winter and NO_x -limited in summer) (Jin and Holloway, 2015; Liu et al., 2010).

Atmospheric aerosols from direct emission and secondary formation can disturb ozone photochemical formation through radiation effects and aerosol heterogeneous chemistry (Li et al., 2017b, 2017c). The modelled surface $\text{PM}_{2.5}$ levels in China decrease substantially by $10\text{--}30 \mu\text{g m}^{-3}$ in 2013–2017 (Fig. S5). Resultantly, the surface O_3 mixing ratios increase broadly by $1.0\text{--}12.7 \mu\text{g m}^{-3}$ on the nationwide average for different seasons by decreasing the negative aerosol effects, particularly in the spring-summer-autumn seasons. Take September for example, in terms of the aerosol effects with decreasing aerosol concentration, the heterogeneous chemical effect ($+11.6 \mu\text{g m}^{-3}$) rather than the aerosol radiative effect ($+1.5 \mu\text{g m}^{-3}$) is the dominant contributor to surface O_3 increase from 2013 to 2017 (Fig. S6). These results partly agree with Li et al. (2019a) using the GEOS-Chem global simulation, who showed that

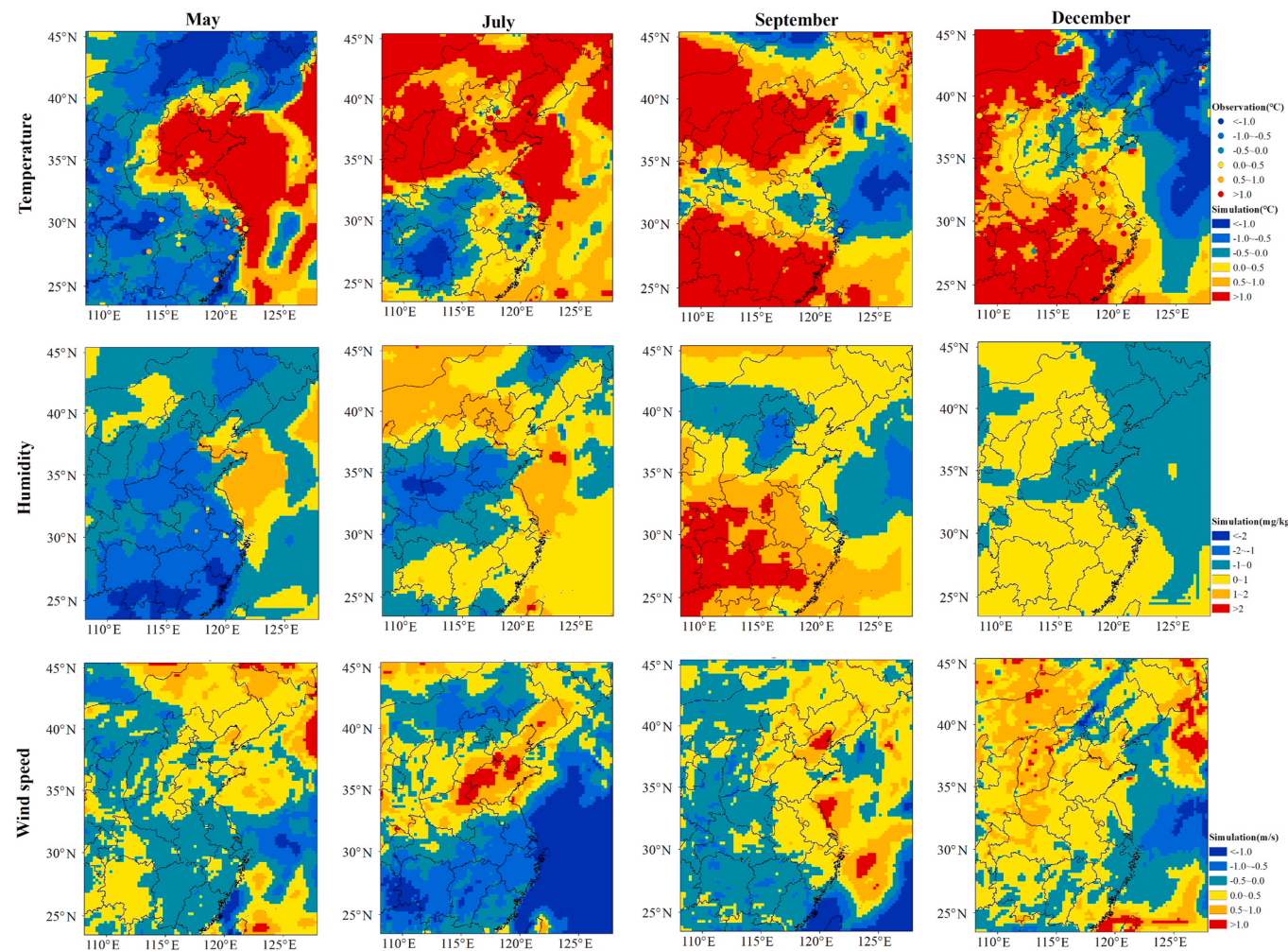


Fig. 9. Modelled changes of surface temperature (upper panels), humidity (middle panels) and wind speed (bottom panels) in May, July, September and December from 2013 to 2017. Observed monthly surface temperature changes are marked with solid circles.

Table 4

Statistical evaluations for the simulated temperature changes ($^{\circ}\text{C}$) in four seasons between 2013 and 2017.

Period	Observation	Simulation	R	MB
May	0.82	0.40	0.83	-0.42
July	0.87	0.60	0.72	-0.27
September	0.85	0.94	0.75	+0.09
December	0.49	0.32	0.66	-0.17

reducing $\text{PM}_{2.5}$ levels in 2013–2017 led to 6–11 $\mu\text{g m}^{-3}$ of summer ozone increase in China by affecting the aerosol heterogeneous chemistry. But our results highlight that in the warm seasons controlling the emissions of NO_x and VOC_s (11–35%) also contributes to surface ozone enhancement in the same degree as the changes in aerosol effects (35–38%), contradicting the conclusions made from Li et al. [2019a]. The discrepancy between our results with Li et al. [2019a] might be caused by the differences in the applied model configurations, chemical algorithms and parameters (Luo and Yu, 2011; Safronov et al., 2019).

The above results highlight the important roles of recent pollutant controls and atmospheric warming in driving the differing regional ozone trends. It indicates that more stringent emission controls and climate adaptation strategies are required to attain the synergetic control of atmospheric particulate matter and ozone in China.

3.3.3. Uncertainties

This study presents a comprehensive analysis of surface ozone trends in China and their influencing factors (i.e., changes in meteorology, NO_x and VOC_s emissions and aerosol effects) in recent years. Nevertheless, some uncertainties still exist in our air quality simulation and assessment.

The MEIC anthropogenic emission inventory in China is compiled based on a bottom-up approach using statistical activity data and emission factors (Li et al., 2017a). This method is of high uncertainty due to the difficulty in gathering detailed activity data, the lag in release of statistical data and the lack of local emission factor measurements. Here, the MEIC inventories in 2012 and 2016 are used as substitutions to quantify the short-term and nationwide emission changes between the years 2013 and 2017. It is estimated that the national emissions for SO_2 , $\text{PM}_{2.5}$, NO_x and VOC_s changed by -53.0%, -31.6%, -22.8% and +0.9% from 2012 to 2016 (MEICv1.3). Zheng et al. (2018) reported that the national emissions of SO_2 , $\text{PM}_{2.5}$ and NO_x in mainland China reduced by 59%, 33% and 21%, respectively, from 2013 to 2017, and the VOC_s emissions increased by 2% for the same interval. The misrepresentation of real emissions changes between 2013 and 2017 may bring some model errors in the chemical simulation.

The effects of aerosol heterogeneous chemistry on ozone depend strongly on the selected uptake coefficients. The ranges of heterogeneous uptake coefficients reported for key atmospheric reactive gases could vary by more than two orders of magnitude, due to the strong dependence on the aerosol composition and mixing state, the hypothetical aerosol surface area, the measurement technique and the

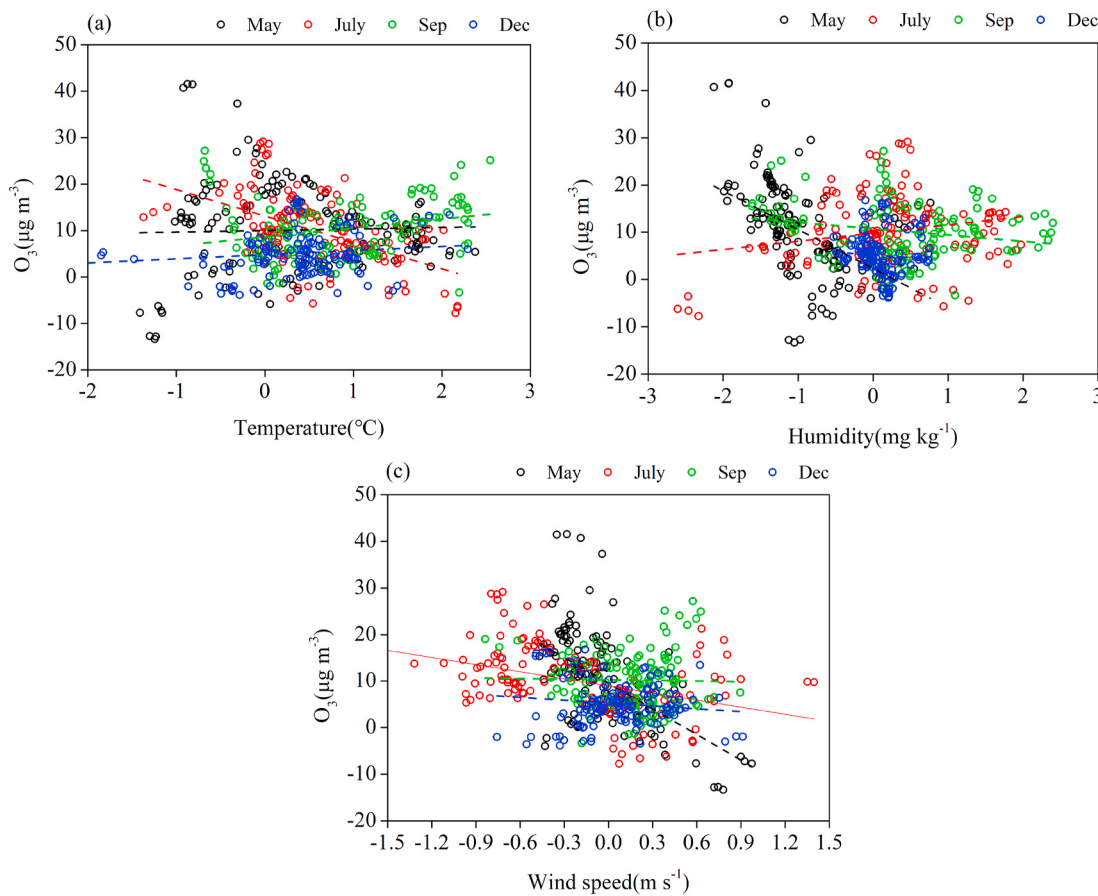


Fig. 10. The relationship of simulated surface O₃ changes to the changes in (a) temperature, (b) humidity and (c) wind speed.

experimental environmental conditions (Ammann et al., 2005; Goodman et al., 2000; Kleffmann et al., 1998; Moise et al., 2002; Rudich et al., 1996; Saathoff et al., 2001; Underwood et al., 2001). We perform an additional sensitivity test, in which the uptake coefficients are assumed to be twofold of those values in Table S1. The simulation shows that the ozone concentration is sensitive to the variations of uptake coefficients, and the surface average O₃ and NO₂ mixing ratios in China change by -8.8% and -1.1% in September when the higher heterogeneous uptake coefficients are used. Li and Han (2011) also estimated that the impacts of the large uncertainties for uptake coefficients on ozone simulation could reach 10.1%. It is essential to assess the importance of uptake coefficients with different ambient conditions in tropospheric photochemistry.

The treatment of boundary layer (PBL) processes also has serious implications for the air quality simulations, which have been evaluated in many studies. Sensitivity experiments using the WRF model (Chen et al., 2017; Hu et al., 2010; Yerramilli et al., 2010) found that the non-local closure YSU scheme produced more realistic temperature, humidity and wind in the lower atmosphere, indicating better simulation of turbulent diffusion than that simulated by the other local closure PBL schemes. Misenis and Zhang (2010) compared the YSU and MYJ PBL schemes in the WRF-Chem model in Houston for a five-day summer episode, and found 20–40% lower PBL height with the MYJ scheme than the YSU scheme, which resulted in higher levels of CO, O₃, and PM_{2.5}. Yerramilli et al. (2012) also indicated that the YSU PBL scheme in combination with Noah land surface model produced better simulations of both meteorology and chemical species than others. Further investigation is needed to evaluate the current PBL scheme in the WRF-Chem air quality simulation.

The other uncertainties in the assessment include the underestimation of PM_{2.5} simulation (Tuccella et al., 2012), the failure to separate

the nonlinear effects caused by emission control and meteorological conditions in numerical experiments (Ansari et al., 2019) etc.

4. Conclusions

The emerging ozone pollution in recent years raises a new challenge to the air pollution control policy in China. Some recent studies have examined the summertime ozone increase in China but presented controversial opinions. Here, we use satellite data and a five-year surface dataset consisting of O₃, NO₂, SO₂ and PM_{2.5} in 74 major cities of China from 2013 to 2017 to document the recent air quality trends, combined with numerical simulations to discuss the possible causes for the observed ozone changes.

The national emissions of NO_x, VOCs, SO₂ and PM_{2.5} change by -22.8%, +0.9%, -53.0% and -31.6%, respectively, during 2012–2016. The decreasing trends for tropospheric PM_{2.5} and NO₂ column concentrations are confirmed by the 5-yr satellite data. The trends of surface air pollutants, e.g., increase in 95th percentile O₃ concentrations, and decreases in PM_{2.5} and SO₂ mean concentrations are uncovered by the analysis, with rates of +1.4~+8.7, -4.0~-7.5 and -2.6~-9.7 $\mu\text{g m}^{-3}$ yr⁻¹ for different seasons across China, respectively. Model efforts find that the attributions of surface O₃ changes in 2017 relative to 2013 vary spatially and seasonally, and that most regions are primarily driven by the changes in anthropogenic emissions (-9.5–47.0 $\mu\text{g m}^{-3}$) rather than meteorological conditions (-8.1–21.3 $\mu\text{g m}^{-3}$). In specific regions and seasons, e.g., south/southwestern and eastern China regions south of 35°N in May and July, the surface O₃ responses to climate variability could be comparable to or even more significant than those due to emission changes. In these major pollution control regions, e.g. northern and mid-eastern China, the recent air pollutant emissions controls show a sinister side-effect on surface ozone changes. The NO_x and VOCs

emissions controls (11–35%) contribute to the surface ozone enhancement in the same degree as the changes in aerosol effects (35–38%) in the warm seasons. We highlight that more scientific and stringent emission controls and climate adaptation strategies are required to attain the synergetic control of atmospheric particulate matter and ozone in different regions of China.

In addition to the aerosol effects on ozone chemistry, the oxidation production of atmospheric aerosols is also closely coupled with photochemical cycle (Meng et al., 1997). Some studies have discussed the impacts of NO_x and VOC_s emissions controls on atmospheric oxidizing capacity and secondary particulate matter production (Nguyen and Dabub, 2002; Pun and Seigneur, 2001). They highlighted that the secondary aerosol production was highly sensitive to the concentrations of atmospheric oxidants, and that in the VOC_s-limited zones the NO_x emission reduction might sometimes lead to an increase of aerosol concentration. Recent evidence from simulations (Geng et al., 2017; Wang et al., 2013) and field observations (Fu et al., 2020) also supported that the persistent heavy aerosol pollution in China was driven by the increased photochemical oxidants. The increasingly serious nitrate and ozone problems have emerged to be the new emphasis of air pollution controls in China (Shao et al., 2018; Wen et al., 2018). Understanding of the nonlinear aerosol and photochemistry feedback is important to resolve the emerging air pollution problems in China.

Data availability statement

The surface air quality data are provided by Chinese National Environmental Monitoring Center (<http://www.cnemc.cn/en/>) and archived at <https://doi.org/10.6084/m9.figshare.12818807.v1>. MODIS AOD is accessible at <https://ladsweb.nascom.nasa.gov>, and OMI TCO and TCN are available from NASA Goddard Space Flight Center (https://acd-ext.gsfc.nasa.gov/Data_services). The surface weather data are accessible at the Integrated Surface Database (<https://www.ncdc.noaa.gov/isd/data-access>). The WRF-Chem model version 3.7 is available at <http://www2.mmm.ucar.edu/wrf/users/downloads.html>. The MEIC data are available at www.meicmodel.org. The NCEP FNL data are accessible at the National Center for Atmospheric Research (NCAR) Research Data Archive (RDA; <http://rda.ucar.edu/datasets/ds083.2/>).

CRediT authorship contribution statement

Mengmeng Li: Methodology, Writing - original draft, Software. **Tijian Wang:** Conceptualization, Writing - review & editing. **Lei Shu:** Software, Supervision. **Yawei Qu:** Software, Supervision. **Min Xie:** Resources, Data curation. **Jane Liu:** Data curation. **Hao Wu:** Validation. **Ume Kalsoom:** Formal analysis.

Declaration of competing interest

The authors declare that they have no known competing financial interests or personal relationships that could have appeared to influence the work reported in this paper.

Acknowledgements

This study is funded by the National Natural Science Foundation of China (41975153, 42077192), the National Key Basic Research Development Program of China (2019YFC0214603, 2020YFA0607802), the Emory University-Nanjing University Collaborative Research Grant, and the Fundamental Research Funds for the Central Universities (14380051, 14380056).

Appendix A. Supplementary data

Supplementary data to this article can be found online at <https://doi.org/10.1016/j.atmosenv.2020.118130>.

References

- Ammann, M., Rossler, E., Strekowski, R., George, C., 2005. Nitrogen dioxide multiphase chemistry: uptake kinetics on aqueous solutions containing phenolic compounds. *Phys. Chem. Chem. Phys.* 7, 2513–2518.
- Ansari, T.U., Wild, O., Li, J., Yang, T., Xu, W.Q., Sun, Y.L., Wang, Z.F., 2019. Effectiveness of short-term air quality emission controls: a high-resolution model study of Beijing during the Asia-Pacific Economic Cooperation (APEC) summit period. *Atmos. Chem. Phys.* 19, 8651–8668.
- Bauer, S.E., Balkanski, Y., Schulz, M., Hauglustaine, D.A., Dentener, F., 2004. Global modeling of heterogeneous chemistry on mineral aerosol surfaces: influence on tropospheric ozone chemistry and comparison to observations. *J. Geophys. Res. Atmos.* 109.
- Bedjanian, Y., Romanias, M.N., El Zein, A., 2013. Interaction of OH radicals with Arizona test dust: uptake and products. *J. Phys. Chem.* 117, 393–400.
- Bloomer, B.J., Stehr, J.W., Piety, C.A., Salawitch, R.J., Dickerson, R.R., 2009. Observed relationships of ozone air pollution with temperature and emissions. *Geophys. Res. Lett.* 36.
- Bulletin, C.E.S., 2013-2017. Chinese Environmental Statistical Bulletin. Ministry of Ecology and Environment of the People's Republic of China, Beijing, China.
- Camarier, L., Cox, W., Dolwick, P., 2007. The effects of meteorology on ozone in urban areas and their use in assessing ozone trends. *Atmos. Environ.* 41, 7127–7137.
- Chen, D.S., Xie, X., Zhou, Y., Lang, J.L., Xu, T.T., Yang, N., Zhao, Y.H., Liu, X.X., 2017. Performance evaluation of the WRF-chem model with different physical parameterization schemes during an extremely high PM2.5 pollution episode in Beijing. *Aerosol Air Qual Res* 17, 262–277.
- Cheng, H.R., Guo, H., Wang, X.M., Saunders, S.M., Lam, S.H.M., Jiang, F., Wang, T.J., Ding, A.J., Lee, S.C., Ho, K.F., 2010. On the relationship between ozone and its precursors in the Pearl River Delta: application of an observation-based model (OBM). *Environ. Sci. Pollut. R* 17, 547–560.
- Chou, M.D., Suarez, M.J., 1999. A Shortwave Radiation Parameterization for Atmospheric Studies, vol. 15. NASA/TM-104606, p. 40.
- Davis, J., Cox, W., Reff, A., Dolwick, P., 2011. A comparison of CMAQ-based and observation-based statistical models relating ozone to meteorological parameters. *Atmos. Environ.* 45, 3481–3487.
- DeMore, W.B., 2000. Chemical Kinetics and Photochemical Data for Use in Stratospheric Modeling JPL, 200.
- Dentener, F.J., Carmichael, G.R., Zhang, Y., Lelieveld, J., Crutzen, P.J., 1996. Role of mineral aerosol as a reactive surface in the global troposphere. *J. Geophys. Res. Atmos.* 101, 22869–22889.
- Ek, M.B., Mitchell, K.E., Lin, Y., Rogers, E., Grunmann, P., Koren, V., Gayno, G., Tarpley, J.D., 2003. Implementation of Noah land surface model advances in the National Centers for Environmental Prediction operational mesoscale Eta model. *J. Geophys. Res. Atmos.* 108.
- Evans, M.J., Jacob, D.J., 2005. Impact of new laboratory studies of NO₂ hydrolysis on global model budgets of tropospheric nitrogen oxides, ozone, and OH. *Geophys. Res. Lett.* 32.
- Fu, X., Wang, T., Gao, J., Wang, P., Liu, Y.M., Wang, S.X., Zhao, B., Xue, L.K., 2020. Persistent heavy winter nitrate pollution driven by increased photochemical oxidants in northern China. *Environ. Sci. Technol.* 54, 3881–3889.
- Gallus, W.A., Bresch, J.F., 2006. Comparison of impacts of WRF dynamic core, physics package, and initial conditions on warm season rainfall forecasts. *Mon. Weather Rev.* 134, 2632–2641.
- Gaudel, A., Cooper, O.R., Ancellet, G., Barret, B., Boynard, A., Burrows, J.P., Clerbaux, C., Coheur, P.F., Cuesta, J., Cuevas, E., Doniki, S., Dufour, G., Ebojje, F., Foret, G., Garcia, O., Granados-Munoz, M.J., Hannigan, J.W., Hase, F., Hassler, B., Huang, G., Hurtmans, D., Jaffe, D., Jones, N., Kalabokas, P., Kerridge, B., Kulawik, S., Latter, B., Leblanc, T., Le Flochmoen, E., Lin, W., Liu, J., Liu, X., Mahieu, E., McClure-Begley, A., Neu, J.L., Osman, M., Palm, M., Petetin, H., Petropavlovskikh, I., Querel, R., Rahpoe, N., Rozanov, A., Schultz, M.G., Schwab, J., Siddans, R., Smale, D., Steinbacher, M., Tanimoto, H., Tarasick, D.W., Thouret, V., Thompson, A.M., Trickl, T., Weatherhead, E., Wespes, C., Worden, H.M., Vigouroux, C., Xu, X., Zeng, G., Ziemke, J., 2018. Tropospheric Ozone Assessment Report: present-day distribution and trends of tropospheric ozone relevant to climate and global atmospheric chemistry model evaluation. *Elementa-Sci Anthropol.* 6.
- Geng, G.N., Zhang, Q., Tong, D., Li, M., Zheng, Y.X., Wang, S.W., He, K.B., 2017. Chemical composition of ambient PM2.5 over China and relationship to precursor emissions during 2005–2012. *Atmos. Chem. Phys.* 17, 9187–9203.
- Goodman, A.L., Underwood, G.M., Grassian, V.H., 2000. A laboratory study of the heterogeneous reaction of nitric acid on calcium carbonate particles. *J. Geophys. Res. Atmos.* 105, 29053–29064.
- Grell, G.A., McKeen, S., Michalakes, J., Bao, J.W., Trainer, M., Hsie, E.Y., 2002. Real-time simultaneous prediction of air pollution and weather during the Houston 2000 field experiment. In: Fourth Conference on Atmospheric Chemistry: Urban, Regional and Global Scale Impacts of Air Pollutants, pp. 224–227.
- Guenther, A., Karl, T., Harley, P., Wiedinmyer, C., Palmer, P.I., Geron, C., 2006. Estimates of global terrestrial isoprene emissions using MEGAN (model of emissions of gases and aerosols from nature). *Atmos. Chem. Phys.* 6, 3181–3210.
- Hu, X.M., Nielsen-Gammon, J.W., Zhang, F.Q., 2010. Evaluation of three planetary boundary layer schemes in the WRF model. *J. Appl. Meteorol. Clim.* 49, 1831–1844.
- Huang, X., Song, Y., Zhao, C., Li, M.M., Zhu, T., Zhang, Q., Zhang, X.Y., 2014. Pathways of sulfate enhancement by natural and anthropogenic mineral aerosols in China. *J. Geophys. Res. Atmos.* 119, 14165–14179.
- Jacob, D.J., 2000. Heterogeneous chemistry and tropospheric ozone. *Atmos. Environ.* 34, 2131–2159.

- Jin, X.M., Holloway, T., 2015. Spatial and temporal variability of ozone sensitivity over China observed from the Ozone Monitoring Instrument. *J. Geophys. Res. Atmos.* 120, 7229–7246.
- Kang, Y.N., Liu, M.X., Song, Y., Huang, X., Yao, H., Cai, X.H., Zhang, H.S., Kang, L., Liu, X.J., Yan, X.Y., He, H., Zhang, Q., Shao, M., Zhu, T., 2016. High-resolution ammonia emissions inventories in China from 1980 to 2012. *Atmos. Chem. Phys.* 16, 2043–2058.
- Kleffmann, J., Becker, K.H., Wiesen, P., 1998. Heterogeneous NO₂ conversion processes on acid surfaces: possible atmospheric implications. *Atmos. Environ.* 32, 2721–2729.
- Lei, W.F., Zhang, R.Y., Tie, X.X., Hess, P., 2004. Chemical characterization of ozone formation in the Houston-Galveston area: a chemical transport model study. *J. Geophys. Res. Atmos.* 109.
- Levy, R.C., Mattoo, S., Munchak, L.A., Remer, L.A., Sayer, A.M., Patadia, F., Hsu, N.C., 2013. The Collection 6 MODIS aerosol products over land and ocean. *Atmos Meas Tech* 6, 2989–3034.
- Li, J., 2020. Pollution trends in China from 2000 to 2017: a multi-sensor view from space. *Remote Sens-Basel* 12.
- Li, J., Han, Z., 2011. A model study of the impact of uncertainty in the heterogeneous uptake coefficients on dust aerosol surface. *Chin. J. Atmos. Sci.* 35, 55–67 (in Chinese).
- Li, K., Jacob, D.J., Liao, H., Shen, L., Zhang, Q., Bates, K.H., 2019a. Anthropogenic drivers of 2013–2017 trends in summer surface ozone in China. *P Natl Acad Sci USA* 116, 422–427.
- Li, L.H., Zhang, Y.L., Liu, Q.H., Ding, M.J., Mondal, P.P., 2019b. Regional differences in shifts of temperature trends across China between 1980 and 2017. *Int. J. Climatol.* 39, 1157–1165.
- Li, M., Liu, H., Geng, G.N., Hong, C.P., Liu, F., Song, Y., Tong, D., Zheng, B., Cui, H.Y., Man, H.Y., Zhang, Q., He, K.B., 2017a. Anthropogenic emission inventories in China: a review. *Natl Sci Rev* 4, 834–866.
- Li, M.M., Wang, T.J., Han, Y., Xie, M., Li, S., Zhuang, B.L., Chen, P.L., 2017b. Modeling of a severe dust event and its impacts on ozone photochemistry over the downstream Nanjing megalopolis of eastern China. *Atmos. Environ.* 160, 107–123.
- Li, M.M., Wang, T.J., Xie, M., Li, S., Zhuang, B.L., Chen, P.L., Huang, X., Han, Y., 2018. Agricultural fire impacts on ozone photochemistry over the Yangtze River Delta region, East China. *J. Geophys. Res. Atmos.* 123, 6605–6623.
- Li, M.M., Wang, T.J., Xie, M., Zhuang, B.L., Li, S., Han, Y., Chen, P.L., 2017c. Impacts of aerosol-radiation feedback on local air quality during a severe haze episode in Nanjing megalopolis, eastern China. *Tellus B* 69.
- Lin, Y.L., Farley, R.D., Orville, H.D., 1983. Bulk parameterization of the snow field in a cloud model. *J. Clim. Appl. Meteorol.* 22, 1065–1092.
- Liu, F., Zhang, Q., Ronald, J.V., Zheng, B., Tong, D., Yan, L., Zheng, Y.X., He, K.B., 2016. Recent reduction in NO_x emissions over China: synthesis of satellite observations and emission inventories. *Environ. Res. Lett.* 11.
- Liu, X.H., Zhang, Y., Xing, J., Zhang, Q.A., Wang, K., Streets, D.G., Jang, C., Wang, W.X., Hao, J.M., 2010. Understanding of regional air pollution over China using CMAQ, part II. Process analysis and sensitivity of ozone and particulate matter to precursor emissions. *Atmos. Environ.* 44, 3719–3727.
- Liu, Y., Gibson, E.R., Cain, J.P., Wang, H., Grassian, V.H., Laskin, A., 2008. Kinetics of heterogeneous reaction of CaCO₃ particles with gaseous HNO₃ over a wide range of humidity. *J. Phys. Chem.* 112, 1561–1571.
- Liu, Y.M., Wang, T., 2020a. Worsening urban ozone pollution in China from 2013 to 2017-Part 1: the complex and varying roles of meteorology. *Atmos. Chem. Phys.* 20, 6305–6321.
- Liu, Y.M., Wang, T., 2020b. Worsening urban ozone pollution in China from 2013 to 2017-Part 2: the effects of emission changes and implications for multi-pollutant control. *Atmos. Chem. Phys.* 20, 6323–6337.
- Lou, S.J., Liao, H., Zhu, B., 2014. Impacts of aerosols on surface-layer ozone concentrations in China through heterogeneous reactions and changes in photolysis rates. *Atmos. Environ.* 85, 123–138.
- Lu, X., Hong, J.Y., Zhang, L., Cooper, O.R., Schultz, M.G., Xu, X.B., Wang, T., Gao, M., Zhao, Y.H., Zhang, Y.H., 2018. Severe surface ozone pollution in China: a global perspective. *Environ. Sci. Technol. Lett.* 5, 487–494.
- Lu, X., Zhang, L., Chen, Y., Zhou, M., Zheng, B., Li, K., Liu, Y., Lin, J., Fu, T., Zhang, Q., 2019. Exploring 2016–2017 surface ozone pollution over China: source contributions and meteorological influences. *Atmos. Chem. Phys.* 19, 8339–8361.
- Luo, G., Yu, F., 2011. Simulation of particle formation and number concentration over the Eastern United States with the WRF-Chem plus APM model. *Atmos. Chem. Phys.* 11, 11521–11533.
- Marchenko, S., Krotkov, N.A., Lamsal, L.N., Celarier, E.A., Swartz, W.H., Bucsela, E.J., 2015. Revising the slant column density retrieval of nitrogen dioxide observed by the Ozone Monitoring Instrument. *J. Geophys. Res. Atmos.* 120, 5670–5692.
- Meng, Z., Dabdub, D., Seinfeld, J.H., 1997. Chemical coupling between atmospheric ozone and particulate matter. *Science* 277, 116–119.
- Misenis, C., Zhang, Y., 2010. An examination of sensitivity of WRF/Chem predictions to physical parameterizations, horizontal grid spacing, and nesting options. *Atmos. Res.* 97, 315–334.
- Moise, T., Talukdar, R.K., Frost, G.J., Fox, R.W., Rudich, Y., 2002. Reactive uptake of NO₃ by liquid and frozen organics. *J. Geophys. Res. Atmos.* 107.
- NBSC, 2004–2016. National Bureau of Statistics of China, Beijing.
- Nguyen, K., Dabdub, D., 2002. NO_x and VOC control and its effects on the formation of aerosols. *Aerosol Sci. Technol.* 36, 560–572.
- Noh, Y., Cheon, W.G., Hong, S.Y., Raasch, S., 2003. Improvement of the K-profile model for the planetary boundary layer based on large eddy simulation data. *Bound-Lay Meteorol* 107, 401–427.
- Pradhan, M., Kyriakou, G., Archibald, A.T., Papageorgiou, A.C., Kalberer, M., Lambert, R.M., 2010. Heterogeneous uptake of gaseous hydrogen peroxide by Gobi and Saharan dust aerosols: a potential missing sink for H₂O₂ in the troposphere. *Atmos. Chem. Phys.* 10, 7127–7136.
- Pun, B.K., Seigneur, C., 2001. Sensitivity of particulate matter nitrate formation to precursor emissions in the California San Joaquin Valley. *Environ. Sci. Technol.* 35, 2979–2987.
- Remer, L.A., Kaufman, Y.J., Tanre, D., Mattoo, S., Chu, D.A., Martins, J.V., Li, R.R., Ichoku, C., Levy, R.C., Kleidman, R.G., Eck, T.F., Vermote, E., Holben, B.N., 2005. The MODIS aerosol algorithm, products, and validation. *J. Atmos. Sci.* 62, 947–973.
- Rogaski, C.A., Golden, D.M., Williams, L.R., 1997. Reactive uptake and hydration experiments on amorphous carbon treated with NO₂, SO₂, O₃, HNO₃, and H₂SO₄. *Geophys. Res. Lett.* 24, 381–384.
- Rudich, Y., Talukdar, R.K., Ravishankara, A.R., 1996. Reactive uptake of NO₃ on pure water and ionic solutions. *J. Geophys. Res. Atmos.* 101, 21023–21031.
- Saathoff, H., Naumann, K.H., Riemer, N., Kamm, S., Möhler, O., Schurath, U., Vogel, H., Vogel, B., 2001. The loss of NO₂, HNO₃, NO₃/NO₂, and HO₂/HOONO₂ on soot aerosol: a chamber and modeling study. *Geophys. Res. Lett.* 28, 1957–1960.
- Safronov, A.N., Shtabkin, Y.A., Berezina, E.V., Skorokhod, A.I., Rakitin, V.S., Belikov, I. B., Elansky, N.F., 2019. Isoprene, methyl vinyl ketone and methacrolein from TROICA-12 measurements and WRF-CHEM and GEOS-CHEM simulations in the far East region. *Atmosphere-Basel* 10.
- Seinfeld, J.H., Pandis, S.N., 2006. Atmospheric Chemistry and Physics: from Air Pollution to Climate Change, second ed. John Wiley and Sons, Hoboken, NJ.
- Shao, P.Y., Tian, H.Z., Sun, Y.J., Liu, H.J., Wu, B.B., Liu, S.H., Liu, X.Y., Wu, Y.M., Liang, W.Z., Wang, Y., Gao, J.J., Xue, Y.F., Bai, X.X., Liu, W., Lin, S.M., Hu, G.Z., 2018. Characterizing remarkable changes of severe haze events and chemical compositions in multi-size airborne particles (PM₁, PM_{2.5} and PM₁₀) from January 2013 to 2016–2017 winter in Beijing, China. *Atmos. Environ.* 189, 133–144.
- Shu, L., Wang, T.J., Han, H., Xie, M., Chen, P.L., Li, M.M., Wu, H., 2020. Summertime ozone pollution in the Yangtze River Delta of eastern China during 2013–2017: synoptic impacts and source apportionment. *Environ. Pollut.* 257.
- Sillman, S., Samson, F.J., 1995. Impact of temperature on oxidant photochemistry in urban, polluted rural and remote environments. *J. Geophys. Res. Atmos.* 100, 11497–11508.
- Silver, B., Reddington, C.L., Arnold, S.R., Spracklen, D.V., 2018. Substantial changes in air pollution across China during 2015–2017. *Environ. Res. Lett.* 14.
- Slade, J.H., Knopf, D.A., 2013. Heterogeneous OH oxidation of biomass burning organic aerosol surrogates compounds: assessment of volatilisation products and the role of OH concentration on the reactive uptake kinetics. *Phys. Chem. Chem. Phys.* 15, 5898.
- Tan, Z.F., Hofzumahaus, A., Lu, K.D., Brown, S.S., Holland, F., Huey, L.G., Kiendler-Scharf, A., Li, X., Liu, X.X., Ma, N., Min, K.E., Rohrer, F., Shao, M., Wahner, A., Wang, Y.H., Wiedensohler, A., Wu, Y.S., Wu, Z.J., Zeng, L.M., Zhang, Y.H., Fuchs, H., 2020. No evidence for a significant impact of heterogeneous chemistry on radical concentrations in the North China plain in summer 2014. *Environ. Sci. Technol.* 54, 5973–5979.
- Thornton, J.A., Jaegle, L., McNeill, V.F., 2008. Assessing known pathways for HO₂ loss in aqueous atmospheric aerosols: regional and global impacts on tropospheric oxidants. *J. Geophys. Res. Atmos.* 113.
- Tuccella, P., Curci, G., Visconti, G., Bessagnet, B., Menut, L., Park, R.J., 2012. Modeling of gas and aerosol with WRF/Chem over Europe: evaluation and sensitivity study. *J. Geophys. Res. Atmos.* 117.
- Underwood, G.M., Song, C.H., Phadnis, M., Carmichael, G.R., Grassian, V.H., 2001. Heterogeneous reactions of NO₂ and HNO₃ on oxides and mineral dust: a combined laboratory and modeling study. *J. Geophys. Res. Atmos.* 106, 18055–18066.
- van der A, R.J., Eskes, H.J., Boersma, K.F., van Noije, T.P.C., Van Roozendael, M., De Smedt, I., Peters, D.H.M.U., Meijer, E.W., 2008. Trends, seasonal variability and dominant NO_x source derived from a ten year record of NO₂ measured from space. *J. Geophys. Res. Atmos.* 113.
- Vukovich, F.M., 1995. Regional-Scale boundary-layer ozone variations in the eastern united-states and their association with meteorological variations. *Atmos. Environ.* 29, 2259–2273.
- Wang, N., Lyu, X., Deng, X., Huang, X., Jiang, F., Ding, A., 2019. Aggravating O₃ pollution due to NO_x emission control in eastern China. *Sci. Total Environ.* 677, 732–744.
- Wang, X., Shen, Z.X., Tang, Z.Y., Li, G.H., Lei, Y.L., Zhang, Q., Zeng, Y.L., Xu, H.M., Cao, J.J., Zhang, R.J., 2020. Characteristics of surface ozone in five provincial capital cities of China during 2014–2015. *Atmosphere-Basel* 11.
- Wang, Y., Zhang, Q.Q., He, K., Zhang, Q., Chai, L., 2013. Sulfate-nitrate-ammonium aerosols over China: response to 2000–2015 emission changes of sulfur dioxide, nitrogen oxides, and ammonia. *Atmos. Chem. Phys.* 13, 2635–2652.
- Wen, L., Xue, L.K., Wang, X.F., Xu, C.H., Chen, T.S., Yang, L.X., Wang, T., Zhang, Q.Z., Wang, W.X., 2018. Summertime fine particulate nitrate pollution in the North China Plain: increasing trends, formation mechanisms and implications for control policy. *Atmos. Chem. Phys.* 18, 11261–11275.
- Xia, Y.M., Zhao, Y., Nielsen, C.P., 2016. Benefits of of China's efforts in gaseous pollutant control indicated by the bottom-up emissions and satellite observations 2000–2014. *Atmos. Environ.* 136, 43–53.
- Yang, G.F., Liu, Y.H., Li, X.N., 2020. Spatiotemporal distribution of ground-level ozone in China at a city level. *Sci. Rep.* 10.
- Yerramilli, A., Challa, V.S., Dodla, V.B.R., Dasari, H.P., Young, J.H., Patrick, C., Baham, J.M., Hughes, R.L., Hardy, M.G., Swanier, S.J., 2010. Simulation of surface

- ozone pollution in the central gulf coast region using WRF/chem model: sensitivity to PBL and land surface physics. *Adv Meteorol*, 319138. <https://doi.org/10.1155/2010/319138>, 2010.
- Yerramilli, A., Challa, V.S., Dodla, V.B.R., Myles, L., Pendergrass, W.R., Vogel, C.A., Tuluri, F., Baham, J.M., Hughes, R., Patrick, C., Young, J., Swanier, S., 2012. Simulation of surface ozone pollution in the Central Gulf Coast region during summer synoptic condition using WRF/Chem air quality model. *Atmos Pollut Res* 3, 55–71.
- Zaveri, R.A., Easter, R.C., Fast, J.D., Peters, L.K., 2008. Model for simulating aerosol interactions and chemistry (MOSAIC). *J. Geophys. Res. Atmos.* 113.
- Zaveri, R.A., Peters, L.K., 1999. A new lumped structure photochemical mechanism for large-scale applications. *J. Geophys. Res. Atmos.* 104, 30387–30415.
- Zeng, G., Pyle, J.A., Young, P.J., 2008. Impact of climate change on tropospheric ozone and its global budgets. *Atmos. Chem. Phys.* 8, 369–387.
- Zhang, Y., Carmichael, G.R., 1999. The role of mineral aerosol in tropospheric chemistry in East Asia - a model study. *J. Appl. Meteorol.* 38, 353–366.
- Zhao, M.F., Xiu, G.L., Qiao, T., Li, Y.L., Yu, J.Z., 2016. Characteristics of haze pollution episodes and analysis of a typical winter haze process in Shanghai. *Aerosol Air Qual. Res.* 16 (7), 1625–1637.
- Zheng, B., Tong, D., Li, M., Liu, F., Hong, C.P., Geng, G.N., Li, H.Y., Li, X., Peng, L.Q., Qi, J., Yan, L., Zhang, Y.X., Zhao, H.Y., Zheng, Y.X., He, K.B., Zhang, Q., 2018. Trends in China's anthropogenic emissions since 2010 as the consequence of clean air actions. *Atmos. Chem. Phys.* 18, 14095–14111.
- Zheng, B., Zhang, Q., Zhang, Y., He, K.B., Wang, K., Zheng, G.J., Duan, F.K., Ma, Y.L., Kimoto, T., 2015. Heterogeneous chemistry: a mechanism missing in current models to explain secondary inorganic aerosol formation during the January 2013 haze episode in North China. *Atmos. Chem. Phys.* 15, 2031–2049.
- Zheng, Y.X., Xue, T., Zhang, Q., Geng, G.N., Tong, D., Li, X., He, K.B., 2017. Air quality improvements and health benefits from China's clean air action since 2013. *Environ. Res. Lett.* 12.
- Zhou, L.H., Zhang, J., Zheng, X.H., Xue, W.H., Zhu, S.G., 2019. Impacts of chemical and synoptic processes on summer tropospheric ozone trend in north China. *Adv Meteorol*, 3148432. <https://doi.org/10.1155/2019/3148432>, 2019.
- Ziemke, J.R., Chandra, S., Duncan, B.N., Froidevaux, L., Bhartia, P.K., Levelt, P.F., Waters, J.W., 2006. Tropospheric ozone determined from aura OMI and MLS: evaluation of measurements and comparison with the global modeling initiative's chemical transport model. *J. Geophys. Res. Atmos.* 111.
- Ziemke, J.R., Chandra, S., Labow, G.J., Bhartia, P.K., Froidevaux, L., Witte, J.C., 2011. A global climatology of tropospheric and stratospheric ozone derived from Aura OMI and MLS measurements. *Atmos. Chem. Phys.* 11, 9237–9251.
- Zoran, M.A., Savastre, R.S., Savastre, D.M., Tautan, M.N., 2020. Assessing the relationship between ground levels of ozone (O_3) and nitrogen dioxide (NO_2) with coronavirus (COVID-19) in Milan, Italy. *Sci. Total Environ.* 740.